Particle Precipitation: Effects on Selected Ionospheric Phenomena

June Lunde

A dissertation for the degree of Philosophiae Doctor

University of Tromsø
Faculty of Science
Department of Physics and Technology

June 2009

ABSTRACT

The motivation behind this thesis has been to study particle precipitation from the Sun into the Earth's upper atmosphere and its effects on selected ionospheric phenomena. Particles from the solar wind can enter the Earth's magnetosphere through magnetic merging, either at the sub-solar point, or at higher latitudes, depending on the configuration of the interplanetary magnetic field. This interaction can be studied from the ground at Svalbard, due to its fortuitous location beneath the magnetospheric cusp region on the dayside, and its location inside the polar cap during night-time. It has been studied how these precipitating particles act on the aurora and ion-acoustic waves in the ionized part of the atmosphere. The studies have been conducted using various methods, including extracting data from databases, running different experiments and building new instrumentation. The latter was a radiation detector for measuring Bremsstrahlung X-rays.

The main instrument used for this study has been the EISCAT (European Incoherent SCATtering) radar located at Svalbard, together with an assortment of other ground based instruments such as photometers, riometers and magnetometers. In addition, particle instruments onboard satellites have been used as well as an X-ray instrument mounted on a balloon launched from Longyearbyen.

Primarily, it is the effect of particle precipitation on large ion-acoustic waves that has been studied. These waves can be observed by advanced radar facilities, both from Svalbard and Tromsø (EISCAT) in the form of spectra known as natural enhanced ion acoustic lines (NEIALs). It has been found that the most energetic particle precipitation causes ion-acoustic waves which mainly propagate downward, while the less energetic part of the particle precipitation is related to ion-acoustic waves which propagate upward.

In this project, large ion-acoustic waves have been discovered during night-time at very high latitudes where they were not expected to occur. Previously, these phenomena have only been observed during daytime at Svalbard. Furthermore, in this work, the infrared atomic oxygen emission line (844.6 nm) has been introduced as a new possible method to detect NEIALs in optical data. Particle precipitation sometimes cause flickering aurora, hence intensity variation and the apparent motion of flickering spots in the aurora have been studied. Finally, precipitating particles typically consists of electrons and ions, and in this study, an example is given on of how the merging of the Earth's and Sun's magnetic fields guide the precipitation.

PREFACE

This doctoral fellowship has been subjected to the University of Tromsø, Faculty of Science, with some instructions; it should be attached to the Cosmic Geophysics group at the Department of Physics and Technology, and directed to research projects where application of the EISCAT (European Incoherent SCATter) radar and in particularly the EISCAT Svalbard Radar is involved. I have followed the latter to accomplish my dissertation.

The required research courses related to the doctorate study were completed at the University Courses on Svalbard (UNIS) during the winter and spring of year 2005. The subjects were "The Upper Polar Atmosphere" and "Radardiagnostic of Space Plasma". In addition, a scientific course about the Magnetosphere Dynamics held in L'Aquila, Italia, was attended in April 2007. From September 2006 until July 2007, an abroad research stay took place in Japan at the Nagoya University as an international co-operation with the Solar-Terrestrial-Environment-Laboratory (STEL).

The PhD work and this doctoral thesis has mainly been carried out at the Auroral Observatory in Tromsø and at Nagoya University in Japan, but contribution and participation in several national (5) and international conferences (8) as well as scientific campaigns (3), have been of invaluable importance and of great value for the study.

Thanks to my supervisor Unni Pia Løvhaug, and to my co-supervisor Dag Arne Lorentzen, who generously undertook guidance for the third time during my higher education. Thanks to all co-authors and contributors in Japan, Italy, USA, Great Britain, Germany, Denmark, Finland, Sweden and Norway who have shared their knowledge and experience with me.

I would like to express my appreciation to the administration and technical staff at the Auroral Observatory for providing good working conditions and facilities. Thanks to Cesar La Hoz and Asgeir Brekke for giving valuable scientific comments to the theory chapter. Thanks to Chris Hall and Hilde Jenssen for proof-reading the manuscript and for pointing out potential ambiguities.

I am thankful to Prof. R. Fujii for inviting me to Nagoya and to Dr. Y. Ogawa for initiating this collaboration. I appreciated the weekly seminars and discussions with the students and researchers at STEL. My special thanks go to Judy, for being a friend and for organising everything so well. You made my stay in Japan so pleasant and memorable for life.

Thanks to all the people who have encouraged and inspired me, in a way that led me to applying for a doctoral fellowship, especially to Kolbjørn Adolfsen, Ulf-Peter Hoppe, Eivind Thrane, Tom-Arild Blix, Arvid Øvergård and Michael Gausa.

Finally, I am most grateful to my brother Thomas, who is always patient and gives unconditional support by listening to my thoughts and worries.

Tromsø, Norway, June 2009

June Lunde

TABLE OF CONTENTS

1. INTRODUCTION

Background

At Svalbard, an incoherent scatter (IS) radar facility is used as a powerful tool to study the Earth's ionosphere and its interaction with the upper polar atmosphere, the magnetosphere and the interplanetary medium by detecting scatter from thermal fluctuations of plasma. Data from the EISCAT Svalbard Radar (ESR) are obtained on a regular basis, either through Common Programmes, or by user-defined experiments. The ESR has been operated since 1996 with a 32 m antenna, and in 1999 the facility was extended with a field-aligned 42 m antenna. Occasionally during measurements, some of the data collected have been reported and termed as naturally enhanced ion acoustic lines (NEIALs). This phenomenon, being observed mainly along the geomagnetic field line, is thus believed to be related to geophysical matters like coherent scatter from destabilised wave activity rather than to technical aspects such as hard targets or space debris. They are typically recognised by a strong enhancement in one or both acoustic shoulders in the ion-line spectrum, and such spectra cannot be explained by ordinary thermal fluctuations. Since the first reported NEIAL event at ESR in 1999, only a few reports exist, and up to 2008, they have all been related to observations in the cusp/cleft region. The terms and conditions to explain this phenomenon are still not clear.

Aim of the Project

The aim of this project is to investigate particle precipitation in the Earth's ionosphere and the geophysical settings with and without occurrences of NEIALs. In particular, NEIAL spectra and their relation to optical aurora are main objectives. The investigation ought to complement already existing findings as well as contribute with new knowledge, see appendix A for illustration. It is especially the electron particle precipitation that will be studied in detail, and might be characterised, whereas its association or/and effects on for instance aurora, Bremsstrahlung X-ray and dispersion, will follow as an implicit aim of this work. A search for NEIAL occurrence other than in the cusp/cleft region is thought to be a valuable task.

Method

In this project, the investigations are based on both old datasets and by participation in scientific campaigns. The ESR has been the primary instrument for all investigations performed. The general philosophy in this thesis is that the method is strengthened by the inclusion of a wide range of ground-based instruments such as Meridian Scanning Photometer, riometer, magnetometers, as well as instruments onboard satellites and a balloon in addition to the IS radar, see appendix B for illustration. Because of this, an open approach with several different attack angles has been chosen.

Old analysed data sets from 1999 until 2005 have been systematically investigated. The data with signatures of NEIAL events have been chosen, and their raw data have been studied step-by-step. It should be noted that data sets with the same experimental code have been given priority, and that supplementary data from other instruments have been studied as well. This study has been the frameworks for Paper I (published June 2007) and Paper V (published May 2009).

In 2005, a combined optical and ESR campaign (iASK) took place from 27 November to 10 December at Svalbard. The scientific results from this campaign can be found in Paper II (published August 2008) and Paper IV (published December 2008). In 2006, a combined satellite and ESR campaign (ESR/REIMEI) took place from 4 January to 9 January and from 30 January to 4 February at Svalbard. The scientific results from this campaign can be found in Paper III (published August 2008). In 2006, a combined balloon and ESR campaign (RDR/BXR) took place from 5 June to 1 July at Svalbard. The operational result from this campaign can be found in the appendix C as a popular science article (published February 2007, in Norwegian only).

Source of Errors

One should always be careful of uncritical comparison of results, especially if the framework condition differs. The best thing to do is to ensure that the conditions are as equal as possible, and if they are not consistent, take that into account. Framework conditions can be divided into two parts; one technical part related to the instrument itself (internal conditions), and one physics part related to nature and time (external conditions). Examples of internal conditions could be temporal and spatial resolution, noise and sensitivity, power and attenuation, frequency and mode-settings, calibration etc. Examples of external conditions can be the geomagnetic location, the time of the day, season variability, solar cycle, geophysical activity and so on. Caution therefore should be applied regardless of whether the measurements compared are from the same instrument, or from different classes of instruments.

Since the ESR is the main instrument used in this study, some awareness of external conditions is mentioned here. In addition, more about the technical aspects can be found in Paper III. In general, the IS-analysis involves the fitting of spectra to raw-data in the form of (ACF) Auto Correlation Function or lag-profiles. Many assumptions are made, such as assuming stationary Maxwellian velocity distributions, so that any drift between electrons and ions are ignored. During disturbed or increased geomagnetic activity this might not be the case. In the presence of significantly large electric fields at high latitudes, the velocity distributions of the plasma become non- Maxwellian, hence the analysis leads to incorrect results. Furthermore, if plasma instabilities such as NEIALs occur, the analysis will fail or show false large electron density and temperatures. If the standard method of analysing ESR data assumes 100% O^+, this could underestimate the ion temperature significantly when there is a mixture of O^+ and NO^+ (e.g., Glatthor and Hermandez). During field-aligned measurements, just as for NEIAL studies, only the parallel ion temperature would be measured. From this, the assumption of Maxwellian distributions is accurate to within 5% for field-perpendicular ion velocities up to 4 km/s (e.g. McCrea et al., 1991). It should also be noted that if any small-scale structures in the velocity component are present in the radar beam, the analysis could overestimate the ion temperature, especially if large velocity changes occur in the plasma.

Finally, it is important to remember that even if an instrument fails to yield an expected result, it should not be used as a proof that the expected outcome does not exist, since it simply could result from the limitation of the measuring technique. Also, even if an instrument measures something distinct as expected at certain conditions, this measurement alone cannot yield a priori results. From this, having one or a few observations of NEIALs during a set of certain conditions, as the case is at the ESR, is not an unambiguous validation and does not exclude other terms or concepts. Nevertheless, all results contribute and are of scientific value.

2. THEORY

In this chapter, some of the basic theory underlying this thesis and ionospheric concepts in general will be briefly discussed. However, theories that are already well described in the published papers, such as NEIALs, ion dispersion and flickering aurora will not be repeated here. This chapter is appropriate to the reader that is not already familiar with topics such as the ionosphere, temperature, plasma, waves in plasma, incoherent scatter technique and particle precipitation. All sections are related to each other, and the transition between them follows a natural order. To keep the text as simple as possible very few formulas have been included, however, almost all formulas related to the theory described can be found in appendix D.

Ionosphere

The ionosphere, in which aurora is displayed, is an atmospheric layer that plays an important role for propagation of radio waves, and it causes signal scintillation and modification of the Earth's current system, both on the ground and in the upper atmosphere. Thus, this layer is able to affect communication systems, navigation, sensitive electronic systems, power plants, electric grids, pipelines and oil surveys. These effects occur because the ionosphere is a region of the Earth's upper atmosphere that consists of partially ionized gases (plasma) mainly caused by solar extreme ultraviolet (EUV) photo-ionization during daylight and X-ray, as well as by impact ionization through energetic particle precipitation. In general, both solar and galactic cosmic rays, as well as energetic charged auroral and radiation belt particles, could ionize the Earth's neutral molecules and atoms. Cosmic rays are extremely energetic (relativistic, close to the speed of light) charged particles (i.e. alpha particles, electrons, and protons) or electromagnetic radiation. They are the most dominating ionizing source below 75 km and consist mostly of alpha particles (4He) and protons (H^+). In fact, all electromagnetic radiation with wavelengths equal to or less than 124 nm (≥ 10 eV) act as ionizing radiation; i.e., it has enough energy to kick out an electron from an atom or molecule. Hence, potential ionizing radiation in the ionosphere is EUV (10 nm – 121 nm), and in particular the strong UV emissions of hydrogen Balmer lines at 121.6 nm (Lyman-α) and 102.5 nm (Lyman-β), soft X-ray (1 nm – 10 nm) and hard X-ray (0.01 – 1 nm), gamma radiation (0.001 – 0.01 nm) and cosmic rays (< 1 pm). Radiation with wavelengths within the middle and upper part of UV (125 nm - 400 nm), visible light (400 nm – 700 nm), infrared (700 nm – 1 mm), micro- (1 mm – 1 m) and radio wave (> 1 m) does not have enough energy to be ionizing. Wavelengths of 100 nm, 1 nm and 0.001 nm correspond to energies of 12.4 eV, 1.24 keV and 1.24 MeV, respectively.

The ionosphere typically starts at 60 km in the mesosphere, continues through the thermosphere, and ends up at about 1500 km in the exosphere, see Fig. 1. However, the boundary layer is not sharp but varies as to whether free thermal (< 1 eV) electrons and ions not bounded to an atom or molecule, are present or not. Moreover, the ionosphere is divided in different regions with the following roughly defined range (Fig. 2); D-region below 90 km, E-region from 90 km to 150 km, and F-region above 150 km. In addition, in daylight, the F-region is divided into F1 and F2 layers as well, which are below and above the maximum plasma density height, respectively. This maximum varies between 200 – 600 km in height, and it is at 300 km on average. Also a third sub-region exists above the F2 peak, namely the upper F-region (> 600 km), also known as the topside ionosphere. Few electrons are produced by the action of the Sun's ionization radiation in the upper F-region, since the neutral density is extremely low in this region. The ionosphere is formed by the ionization of atmospheric gases, in particular N_2, O_2 and O.

The dominant positive ions in the D-region are molecular NO^+ and O_2^+, but also negative ions such as CO_3^-, NO_3^- and Cl^- are present. In the E-region, it is the N_2^+, NO^+ and O_2^+ that dominate, and O^+ is dominant in the F-region. The upper F-region, by definition, ends where O^+ decreases and H^+ begins to be the dominant ion species. The ion production rate increases with ionization, and the loss terms that dominate are: i) photochemical or chemical processes like attachment, radiative- and dissociative recombination in the F1-region and below, ii) the transition between chemical processes and diffusion in the F2-region, iii) and transport such as diffusion and convection in the upper F-region. Since the collision frequency decreases proportional with the neutral density, the diffusion is important at greater heights.

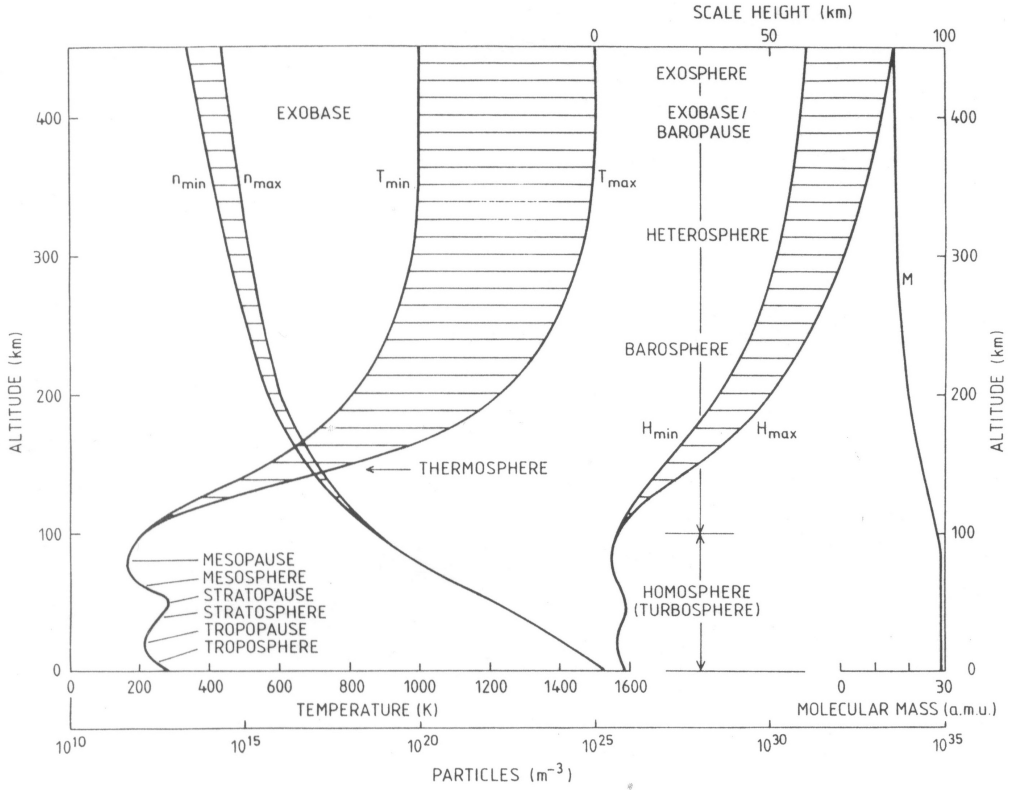

Fig. 1. Model height profiles of the temperature T, density n, molecular mass M, and scale height H in the Earth's atmosphere below 450 km. The different regions are indicated by their characteristic names according to temperature or composition. The variability in the different parameters with respect to solar activity is indicated by the hatched areas. (From Brekke, 1997, in Physics of the Upper Polar Atmosphere.)

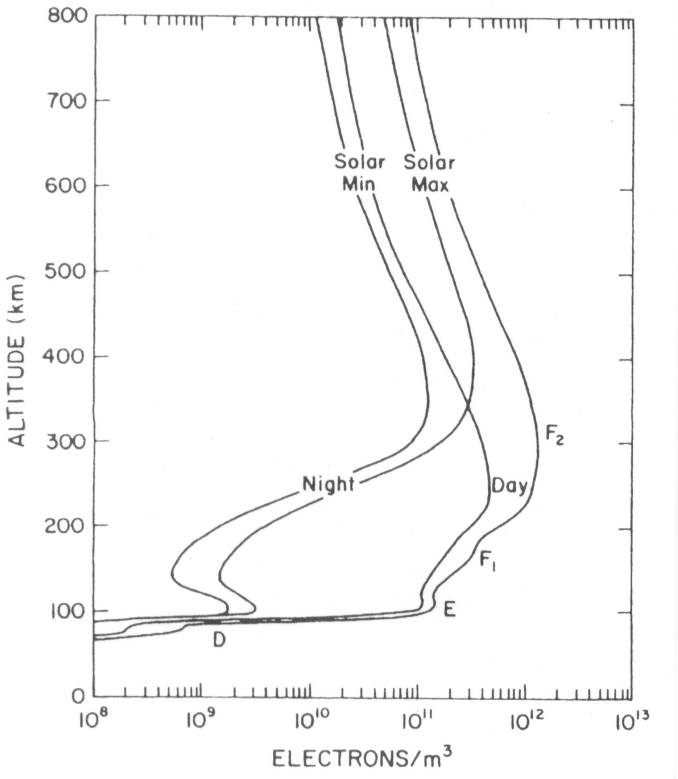

Fig. 2. Typical midlatitude ionospheric electron density profiles for sunspot maximum and minimum conditions at daytime and night-time. The different altitude regions in the ionosphere are labelled with appropriate nomenclature. (From Richmond, 1987, in The Solar Wind and the Earth.)

Only 1% of the atmospheric mass (5.27 x 10^{18} kg) lies above 30 km and only 0.001% above ~80 km. Thus, the ionosphere represents less than 0.1% of the total mass of the Earth's atmosphere. At sea level the atmospheric density is about 1.3 kg/m^3, while at 300 km it is reduced to only 10^{-12} kg/m^3 (10^{-11} kg/m^3) during average solar flux and solar minimum (maximum). The number density (all species) of the atmosphere decreases monotonically with height from 10^{25} m^{-3} at ground level to 10^{15} m^{-3} at 300 km and 10^{10} m^{-3} at 1000 km. The ratio of charged particles to neutral particle concentration varies between 10^{-8} at 100 km and 10^{-1} at 1000 km during daytime, whereas at the typical height of maximum plasma density (~300 km), the ratio is 1 electron per 10 thousand neutrals (10^{-4}). The electron density varies with height, and depends on the time of day, season, sun-spot number and degree of disturbed ionosphere. Typical electron densities at high latitudes during day and night are less than 10^{10} m^{-3} in the D-region, 10^9 - 10^{11} m^{-3} in the E-region, and 10^{10} - 10^{12} m^{-3} in the F-region, see Fig. 3. Absence of sunlight generally causes less density, but despite a smaller solar zenith angle in summer the electron density is higher during winter than summer above about 200 km. The latter is due to seasonal anomaly, which occurs because of seasonal changes in the neutral atmosphere. The O/N_2 ratio increases and decreases in the winter and summer hemispheres, respectively. This results in a higher O^+ density in the F-region altitudes during winter time. In the presence of nighttime aurora the density at about 120 km could reach some 10^{12} m^{-3} within a few tens of seconds.

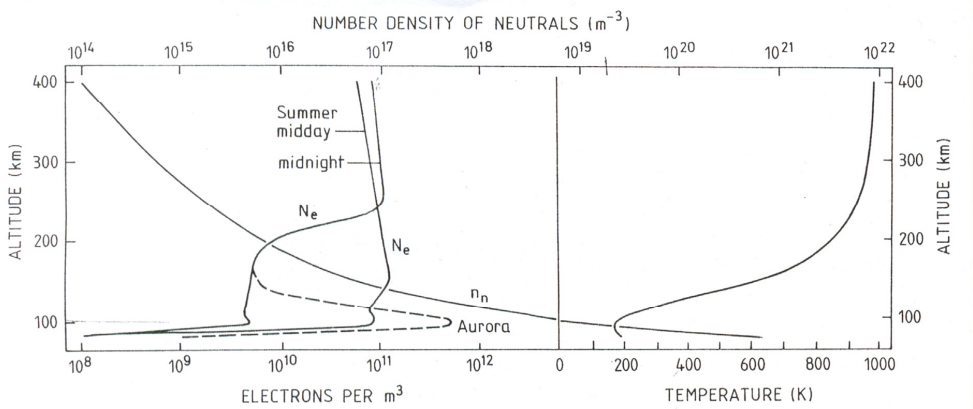

Fig. 3. An electron density profile represents the average daytime and night-time conditions at high latitudes. The dashed line indicates the density profile for auroral conditions. The background neutral density profile together with an average neutral atmosphere temperature profile is also schematically illustrated. (From Brekke, 1997, in Physics of the Upper Polar Atmosphere.)

Both the pressure and collision frequency (υ) decrease with height, and in the exosphere (> 600 km), the typical distance an individual thermal particle can travel in the horizontal direction before the statistical probability for collision with another particle or interacting with a wave is imminent, becomes equal or greater than the scale height (> 60 km). In comparison, the mean free path below the exosphere is about 1 km at 200 km, ~10 m at 140 km, ~1 m at 120 km and ~0.001 m at 60 km. From this, increased neutral density increases the collision frequency between ionized species and neutrals. These collision frequencies act differently on electrons and ions, hence they play an important role in partially ionized plasma regarding the ionospheric electric currents below 120 km. Above about 180 km, the plasma is fully ionized, and the collision frequencies of charged particles with neutrals are much less than the plasma frequency ($f_p >> \upsilon$), thus the charged particles do not "see" the neutrals. The collision frequency between electrons and neutrals (υ_{en}) is typically a factor 10 higher than between the ions and neutrals (υ_{in}). The former is about 500 Hz at 200 km. As the Earth's magnetic field strength increases further down in the ionosphere, the gyro/Larmor radius and the gyro/cyclotron frequency of a charged particle decrease and increase, respectively. From this, charged particles are in general controlled by the magnetic field. However, the circular motion in a uniform magnetic field does not change the particle's kinetic energy. Furthermore, the gyro radius (r_g) increases with increasing energy or mass, while the gyro frequency (f_g) decreases with increasing mass. Energies of 10 keV (1 eV) coincide with electron gyro radius of 6.7 m (6.7 cm), ion gyro radius of 1.2 km (12 m) for O^+ and 290 m (29 cm) for H^+. A representative gyro frequency would be 1.4 MHz, 48 Hz and 786 Hz for electrons, O^+ ions and H^+ ions, respectively.

The gyro frequency is important in relation to how the ions and electrons act in the E-region. If the ion collision frequency is larger than the ion gyro frequency ($\upsilon_{in} >> f_{gi}$), the ions are not magnetized, and if, at the same time, the electrons are magnetized as the electron collision frequency is less than the electron gyro frequency ($\upsilon_{en} << f_{ge}$), they could cause an enhanced electric current in the E-region, known as the electrojet. In the F-region, the collision frequency is always less than the gyro frequency ($\upsilon << f_g$), while in the D-region, the collision frequency is always greater than the gyro frequency ($\upsilon >> f_g$). Charged particles that are not magnetized, such as in the D-region, will thus follow the

neutral wind with the same velocity, while in the F-region, the charged particles will follow the electrodynamic drift (E x B), so that only the component of neutral wind along the magnetic field line could have an effect on the plasma drift. From this, the neutral wind is almost a negligible factor in the F-region above ~180 km, while below and in the E-region it should be taken into account and in the D-region it must be. Finally, it should be noted that beside the electrojets, ionospheric currents in general exist as long as the charged particles drift with different velocities. Above 250 km or so, the electrons and ions are typically drifting with the same velocity, thus no current.

Temperature

Temperature can be defined in different ways due to different degrees of freedom – otherwise the definition of temperature is the same for all matter (i.e. fluids, solid matter, gas and plasma): temperature is the energy related to random motion. There are several kinds of random motion: translational, rotational and vibrational, and each one contributes with different degrees of freedom to the determination of the temperature in thermal equilibrium. Each degree (N) of freedom contributes with (N k_B T)/2 to the total energy, where T is the temperature, k_B is Boltzmann's constant and N is typically 3 in plasma physics applications (F-region and topside). In the ionosphere, the temperature (thermal energy) of a particle is directly proportional to average random kinetic (translational) energy and the neutral temperature will in general increase dramatically above the mesospause (~80 km) into the thermosphere, until it reaches an overall maximum of about 1000 K. However, the maximum and minimum of the neutral temperature depend on time, latitude, solar activity and luminance. Typically, between midnight and noon during solar minimum (maximum), the temperature varies between ~740 (1000) – 1300 (1700) K, see Fig. 4.

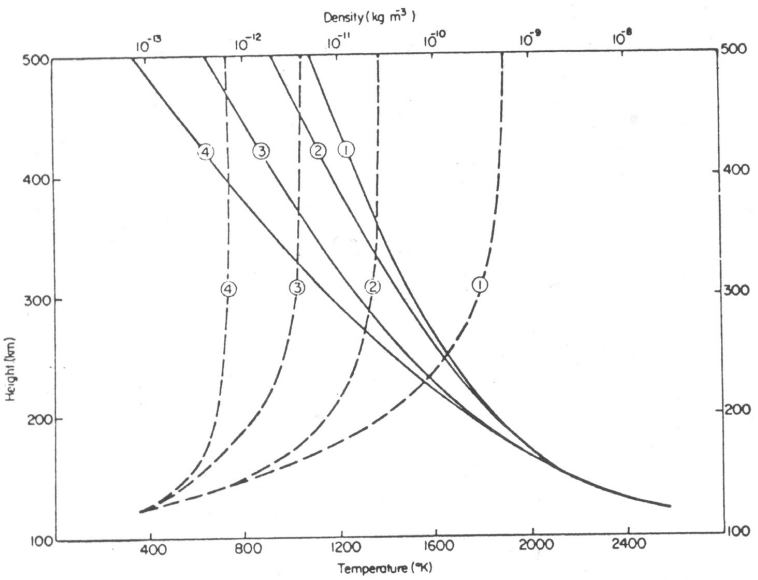

Fig. 4. Vertical distribution of density and temperature for high solar activity at noon (1) and midnight (2), and for low solar activity at noon (3) and midnight (4), according to the COSPAR International Reference Atmosphere (1965). (From Hargreaves, 1992, in The solar-terrestrial environment).

The neutral temperature maximum will typically occur at about 400 km, in the region called exobase, and then the temperature becomes constant with altitude in the exosphere. In the exosphere (> 600 km), individual atoms have the possibility to escape from the Earth's gravitational attraction if the temperature is high enough. The background exospheric temperature is normally between 1000 and 1500 K, too low to escape, but if the temperature increases, so will the velocity, and the minimum escape velocity is about 9.7 km/s at 2000 km. This is somewhat less than the escape velocity at the Earth's surface, which is ~11.2 km/s. In general, it requires a huge temperature for O and He to escape. A factor 16 and 4 more than for H is related to O and He, respectively, and the escape temperature is equal to or greater than 4900 K (>0.63 eV) at about 500 km. Thus the escape velocity (~11 km/s) is more than twice the mean thermal velocity (4.98 km/s) of atomic hydrogen at a temperature of 1000 K.

In the ionosphere, different temperatures of electrons, ions and neutrals can exist, see Fig. 5, and during geomagnetic quiet conditions at altitudes larger than 110 km, the relation between the electron temperature (T_e), the ion temperature (T_i) and the neutral temperature (T_n) is typically: $T_e \geq T_i \geq T_n$. The mass difference between an electron and a neutral is huge. Hence, it is much easier for the electron to depart from the thermal equilibrium with decreasing electron to neutral collision frequency than correspondingly for ions. The electrons are heated by photo-electrons created by UV solar radiation, while ions are heated by electrons. Since the electron heating rate is larger than the electron to ion heat transfer, this cause $T_e > T_i$. It is the electron heat conduction that determines how much larger T_e will be than T_i. However, during disturbed geomagnetic conditions, the ion temperature can get higher than the electron temperature at about 120 km, due to heating caused by a strong electric current ($\geq 10^6$ A). Above about 150 km altitude, the electron temperature is typically twice as high as the ion temperature ($T_e \approx 2*T_i$), and the ion- and electron temperature increase from 650 - 1500 K and 1300 – 3500 K, respectively, until reaching the topside ionosphere. At lower altitudes, below 110 km, the electron- , ion- and neutral temperatures are forced into a state of thermal equilibrium ($T_e \approx T_i \approx T_n$) by a very high collision frequency between charged and neutral particles.

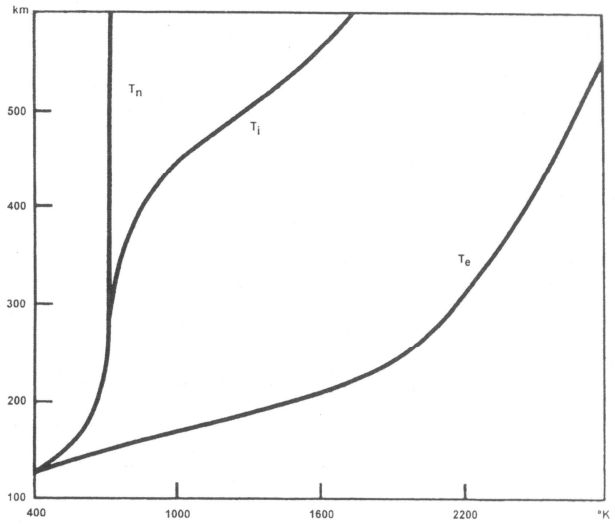

Fig. 5. Representative altitude profiles between 120 and 600 km of the neutral- (T_n), ion- (T_i), and electron temperatures (T_e). (From Giraud and Petit, 1978, in Ionospheric Techniques and Phenomena.).

It is the balance between the heating and cooling rates that decides the temperatures in the ionosphere. An example of cooling sources is inelastic- and elastic collisions between the charged and neutral particles, in which the thermal energy is transferred from the charged particles to the neutral particles. As an example, ion-neutral collisions are elastic while electron-neutral and electron-ion (Coulomb) collisions are inelastic. In the former, the energy, mass and momentum of the colliding particles are conserved in the collision process (no energy is lost), while in the latter this is not the case. Ion-neutral collisions are usually elastic because ions have a thermal energy which is insufficient to excite internal degrees of freedom. On the other hand, electron-neutral collisions can be inelastic when the electrons are photo-electrons (also called suprathermal) with enough energy to excite internal degrees of freedom, such as ionization, chemical reactions and electron excitation. Also rotational, vibrational and fine structure excitations have a cooling effect on the thermal electron population, but the Coulomb collisions with the ambient ions are the dominant energy loss mechanism for the electrons. The latter means that the (thermal) electrons receive more energy from the photo-electrons than they can transfer to the ions, therefore the electrons are hotter. How hot, is determined by the electron thermal loss due to thermal conduction. Thermal electron energy transfer to the neutrals is negligible due to the mass difference and low collision frequency. Absorption of EUV and X-ray radiation is the dominant heating source in the ionosphere, which corresponds to a global mean heating rate at ~0.5 mW/m^2. However, heating through Joule heating and particle heating from energetic charged particles are of particular importance at high latitudes. The particle heating rate is found to be roughly 30% of the particle energy flux (Hays et al., 1973), and it is proportional to the electron density squared, while the Joule heating is found by e.g. looking at the deviation in the horizontal component (ΔH, corrected due to quiet conditions) from the magnetometer (Duboin and Kamide, 1984). Joule heating occurs mostly in the auroral region, and is typically stronger in dawn than dusk. Another heat source, thought less important, is the dissipation of tidal motions and gravity waves by turbulence and molecular viscosity.

More specific examples of heating sources are particle precipitation (i.e. electrons and protons) that heats the electrons efficiently above 150 km, and auroral electrons that heat the ionosphere mainly between 100 and 130 km (a maximum at ~120 km). Solar illumination heats all species, electrostatic plasma waves caused by large electron to ion relative drift velocities (current) heats up the electrons around 110 km, and strong electric fields that enhances the ionospheric electric currents which produce Joule heating. Joule heating is a local heating due to collisions between the neutrals and the ions, caused by a dissipative current parallel (Pedersen) to the electric field, which in particular acts on ions, but both the ion and neutral temperatures increase. This also causes temperature enhancement in the F-region because of upward winds and N_2 density depletion. Furthermore, the Joule heating is proportional with the total electric field squared and thus increases largely with increased electric field, and it is proportional to the Pedersen conductivity which increases with increased electron density. Strong perpendicular electric fields enhance anisotropic plasma below 300 km which subsequently enhances the ion temperature. Currents which are perpendicular to the electric field (Hall) do not contribute to heat dissipation. In general, Pedersen and Hall currents dominate above and below 120 km, respectively. Finally, both solar EUV radiation and auroral precipitation give rise to suprathermal electrons in the ionospheric plasma.

Plasma

Plasma in nature is an unbound (in laboratory it can be bounded) ionized gaseous state which consists of free positively and negatively charged particles which act collectively, it is quasi-neutral in the stationary state with equal charge density on a macroscopic level, and each species has its own plasma frequency. The plasma frequency is lower for heavier particles, and the natural electron plasma frequency (f_{pe}) between 200 - 500 km could vary between 1.8 – 18 MHz (corresponding to density values between 4E10 – 4E12 m^{-3}), but more typical values at high latitudes would be around 10 MHz and 3 MHz at about 250 km and 150 km, respectively. Being quasi-neutral means that the plasma contains approximately the same amount of positive ions and negative electrons whereby, on average, there is no net charge. For a particle to be considered as a free particle, its typical potential energy related to its nearest neighbour must be much smaller than its random kinetic (thermal) energy. More than 99% of all known matter is in the plasma state. In the universe, plasma is abundant, and includes galaxies, stars and the Sun. In the Earth's upper atmosphere and near the Earth's surface, natural plasma also exists in the form of aurora and lightening strokes. Plasma can be produced by strong heating (a few thousand K) of an ordinary gas until the molecule's energy exceeds the ionization energy, or the gas could be exposed to energetic electromagnetic radiation like X-ray or extreme UV light. If the gas is rarefied within vacuum chamber, less power (and temperature) is required to ionize the gas, and ions can be produced by for example injecting fast electrons which then knock other electrons off the neutral gas molecule. The simplest example of plasma in daily life is fluorescent tubes as well as plasma displays.

Each particle in a plasma tries to build up its own shielding cloud, and in order for a plasma to be quasi-neutral, the physical dimension of the system must be large compared to the Debye length. The Debye length corresponds to the distance over which a balance is obtained between the thermal particle energy, which tends to perturb the electric neutrality, and the electrostatic potential energy resulting from any charge separation, which tends to restore charge neutrality. Thus, the random kinetic energy must be greater than the average electrostatic potential energy, and the Debye length is the minimum distance over which a plasma can exhibit collective behaviour. This means that for a plasma phenomenon that varies over scale lengths less than (or within) the Debye length, the plasma may not be neutral and the ions and electrons can be treated as individual particles. The Debye length increases with increased temperature and decreases with increasing density, thus in the ionosphere from D- region up to the peak F-region, the Debye length decreases with height. This is opposed to the scale height that increases with height, since both the pressure and collision frequency decrease with increasing height. Actually, because the plasma density decreases more slowly with height than the neutrals, the isothermal scale height for plasma is twice as large compared to the neutral atmosphere (~8.4 km at sea level, 288 K, and ~10.5 km at 120 km, 360 K). A typical scale height for plasma at 200 km would be about 46 km, about 66 km at 600 km and it varies between 170 km and 620 km above 1000 km. The typical Debye length is ~1 cm in the D-region and few mm in the F-region. In contrast, above the peak F-region, the Debye length increases with height, as the temperature increases and the density decreases, thus it varies between 10 m (magnetopause) and 400 m (tail-lobe) in the magnetosphere. Figure 6 shows the principle of plasma.

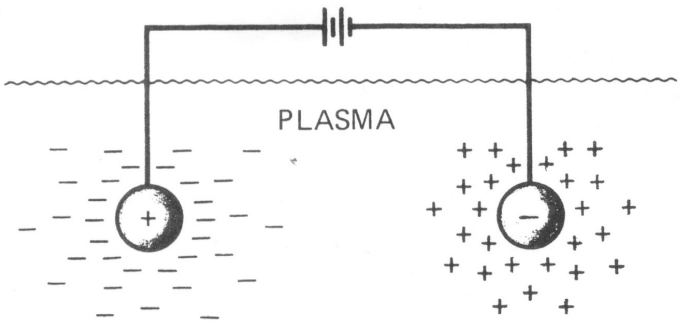

Fig. 6. An illustration of the behaviour of a plasma and its ability to shield out electric potentials that are applied to it, Debye shielding. (From Chen,1984, in Introduction to Plasma Physics and Controlled Fusion.)

Every plasma in equilibrium and non-equilibrium contains certain levels of fluctuations, which depends entirely on the temperature of the plasma due to the thermal motions of its particles. It should be noted that the kinetic temperature of a plasma is not necessarily a true temperature in the thermodynamic sense, since it requires that the plasma is in, or close to, thermal equilibrium. For a cold plasma, the ratio between the kinetic- and magnetic pressure is much less than 1 ($\beta << 1$), while it is equal or greater than 1 for warm plasma ($\beta \geq 1$). The solar wind is a typical warm plasma while ionospheric plasma is mostly cold. Also, sometimes the plasma is divided by thermal energy, in such a way that energies less and greater than 10 eV represent cold and hot plasma, respectively. The degree of plasma ionization such as weakly-, partially- and fully ionized plasma is determined through which types of collisions dominate. In weakly ionized plasma it is only the ion-neutral and electron-neutral collisions that need to be considered, while collisions between charged particles (Coulomb) can be neglected. In partially ionized plasma however, all collisions between ions, electrons and neutrals have to be taken into account. In a fully ionized plasma the ion-neutral and electron-neutral collisions are negligible while it is the long-range nature of Coulomb interactions that dominates.

The Earth's ionosphere below the F-region is not fully ionized, since the amount of neutral collisions with ions and electrons is considerable in both the E- and D-regions. The collision frequency is thus comparable to or larger than the plasma frequency. However, above about 200 km the ionospheric plasma can be considered as fully ionized because the plasma frequency is much larger than the electron and ion collision frequencies. The charged particles do not have contact with neutrals, except in some phenomena where the ion-neutral collisions are important, such as Joule heating in the F-region. However, if the charged particles collide too often with neutrals, the electrons will be forced into equilibrium with the neutrals, and the medium becomes a neutral gas, not a plasma anymore. At least this happens at night when there is no ionization source (no UV radiation, except for energetic particles at high latitudes). The criteria for an ionized medium to behave as a plasma can be summarised as follows: i) the physical dimension of the system must be large compared to the Debye length, ii) the plasma inside a Debye sphere must contain enough particles, and iii) for the electron to remain unaffected by collisions with the neutrals, the average time between two electron-neutral collisions must be much larger than the reciprocal of the plasma frequency. The latter means that the electron-neutral collision frequency must be much smaller than the plasma frequency ($\upsilon_{en} << f_{pe}$).

Waves in Plasma

In general, there are 3 main types of waves in plasma: i) Electrostatic waves, ii) Electromagnetic waves, and iii) Low-Frequency Magnetized Plasma waves (e.g. Alfvén or magnetosonic waves). The low frequency magnetized plasma waves have to consider both the ion and electron motions. Electrostatic waves can be divided into a high frequency electrostatic plasma wave, the Langmuir wave, and a low frequency electrostatic plasma wave, the Ion-Acoustic wave. These two waves do not have a wave magnetic field, while the electromagnetic wave (e.g. light wave, whistler wave) has. The latter can only propagate through unmagnetized plasma if the frequencies are higher than the plasma frequency. In general, in a wave motion, the energy oscillates in different ways depending of what type of wave: i) in a Langmuir Wave the energy exchange is between kinetic particle and electric field energies, ii) in Ion-Acoustic Waves the energy exchange is between kinetic and potential energies and iii) in Alfvén Waves the energy exchange is between kinetic and magnetic field energies. An overview of different types of waves in magnetized plasma is given in Fig. 7, while Fig. 8 illustrates the dispersion relation of waves in unmagnetized uniform plasma.

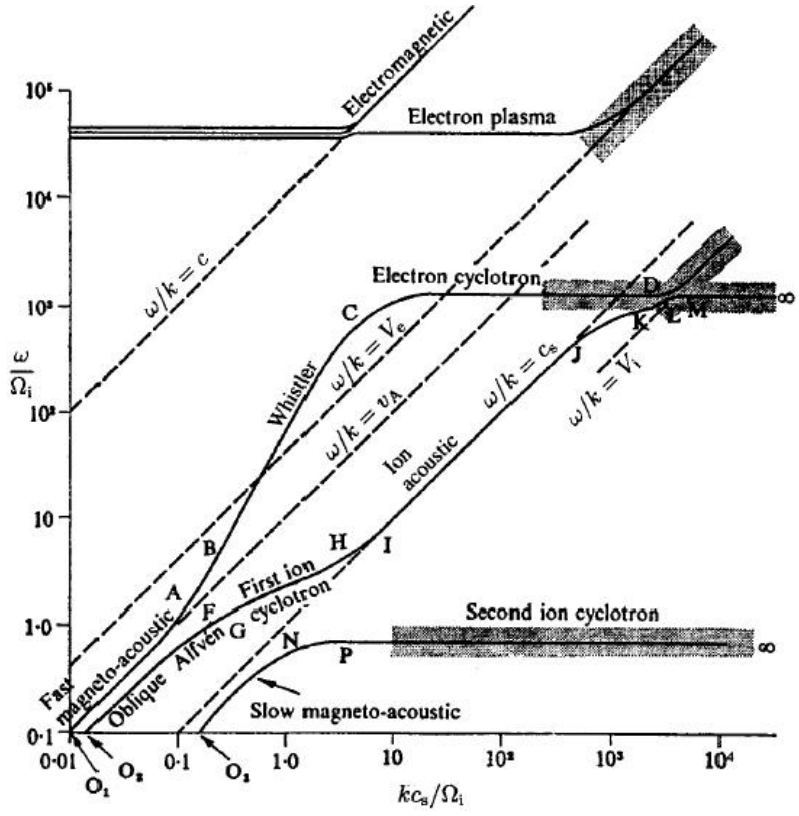

Fig. 7. Dispersion curves for oblique waves in low β plasma with electron cyclotron frequency (Ω_e) less than the plasma frequency (ω_{pe}). The annotations seen in the figure corresponds to dispersion relation (ω/k), Alfvén speed (v_A), Ion-Acoustic speed (c_s), Light speed (c), Electron thermal speed (V_e) and Ion thermal speed (V_i). The capital-letters correspond to different modes. (From Boyd and Sanderson, 2003, in The Physics of Plasmas).

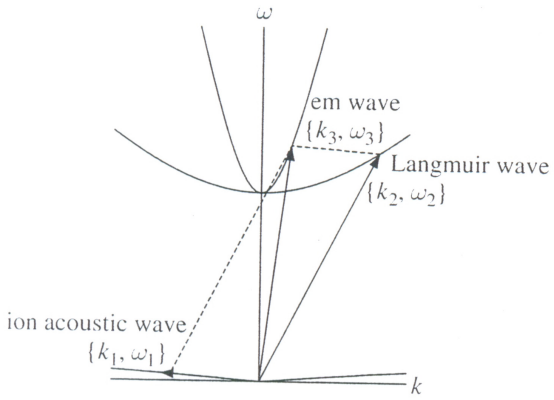

Fig. 8. Electromagnetic wave decaying into a Langmuir wave and an ion-acoustic wave. The ion-acoustic wave propagates backwards in order to have ω_3 (k_1 + k_2) = ω_1 (k_1) + ω_2 (k_2). (From Bellan, 2006, in Fundamentals of Plasma Physics.)

Whenever plasma is being disturbed, the electron will start to oscillate with a certain plasma frequency. This oscillation will later on decay due to damping effect from collisions. A spatially localized perturbation in cold plasma will not propagate at all, but will oscillate at the plasma frequency, but if the pressure is included like in warm plasma, this will result in a propagating wave, which is known as Electron plasma wave or Langmuir wave [MHz]. Electrons in thermal motion carry information into neighbouring regions about what is going on in the oscillating region. If the damping of this wave is total, only a resonance peak is left, corresponding to the plasma frequency. Thus, the Langmuir wave has a frequency close to the resonance frequency of the cold plasma, of which the particles are initially at rest, with no random thermal velocities. In the framework of the incoherent scattering of radio waves, the width of the plasma lines depends on the damping of the Langmuir wave. The frequency of the Langmuir wave increases with increasing electron density, therefore the frequency of the down-shifted and up-shifted plasma lines increases with increasing plasma density. In Langmuir waves, the ions are too heavy to respond, it is only the electrons which contribute to this wave.

On the other hand, the ions have an important role in Ion-Acoustic waves [kHz], since they control the electrons even though they are not involved in the radar backscattering itself. This wave is analogous to sound waves in neutral gas, as they both propagate longitudinally, but an important difference is that the Ion-Acoustic wave includes electrostatic forces. Thus, this wave occurs over a wide range of wavelengths and propagates in any direction in an unmagnetized plasma and along the magnetic field in a magnetized plasma (the same propagations apply for a Langmuir wave). The amplitudes of the electron and ion oscillations are not quite the same, and the resulting Coulomb force provides the potential energy to drive the waves. The Ion-Acoustic frequency is proportional to the square root of the ion temperature divided by the ion mass, and since the ion temperature increases with height, so does the ion acoustic frequency. The ions have a damping effect on the Ion-Acoustic wave. If these waves are heavily damped, the incoherent scatter spectra will broaden. This is also the case if a thermal motion occurs. If the wave gains more energy from electrons than it loses to electrons, the Ion-Acoustic wave will grow. The temperature ratio between electrons and ions in plasma can vary, which causes different behaviour. If i) $T_e/T_i \approx 1$, the Landau damping is strong because the phase velocity of the Ion-Acoustic mode is comparable to the ion thermal speed, ii) $T_e/T_i = 2$, an Ion-Acoustic wave can propagate with less Landau damping, and iii)

$T_e/T_i>3$, the Landau damping becomes even weaker because the phase velocity becomes much greater than the ion thermal speed. If a beam in the velocity distribution function is present, this could cause instability, since with a beam, there are more particles that move slightly faster than the wave than particles moving slightly slower. The faster ones will give more energy to the wave than the energy slower particles will absorb. Thus the wave will gain energy and grow. However, for this to happen, the beam has to produce a current strong enough to excite instability.

The Alfvén wave is a basic magnetohydrodynamic (MHD) wave, which propagates along the direction of the magnetic field and whose displacement is transverse to it. This wave is thought to be generated by the Kelvin-Helmholtz instability process, which results when a magnetospheric plasma streams over another one. The combination of mechanical (pressure) and electromagnetic forces (charged particles) gives rise to different types of MHD waves, and the damping of these waves in the ionosphere depends on the density of the neutral as well as the charged particles. MHD waves have lower frequency than the plasma frequency, and the latter is greater than the gyro (cyclotron) frequency, $f_{MHD} < f_g < f_p$. If both the electric- and magnetic fields are neglected while the pressure dominates we are talking about sound waves, if only the pressure are neglected while the electric- and magnetic field dominates we are talking about cold plasma waves, and finally, without neglecting any, we are talking about warm plasma waves. Waves in cold uniform magnetized plasma occur in the ion- and electron cyclotron mode, which can lead to whistler waves, which can be caused by lightning. Electron whistler waves can be observed from the ground while ion whistler waves (proton or helium) not. Electron whistler waves are recognised by a high frequency (~ 1 - 30 kHz) which decrease in frequency with time (1 second), while an ion whistler is recognized by one or more slowly rising tones (~ 1 - 500 Hz) lasting for several seconds. The electron cyclotron frequency is the characteristic wave frequency in magnetized plasma. At extremely low frequencies both whistlers and ion-cyclotron waves become Alfvén waves.

Possible wave modes in magnetized plasma are (Fig.9): i) Fast magnetosonic mode, ii) Slow magnetosonic mode and iii) Transverse (shear) Alfvén mode. However, some wave products from fast magnetosonic mode and shear Alfvén mode are also possible in cold plasma. In the magnetosonic modes, the plasma pressure is represented through the sound speed (longitudinal propagation) and the magnetic field is represented through the Alfvén speed (transverse propagation). Thus, in contrast to the shear Alfvén mode, which propagates parallel to the ambient magnetic field and is purely transverse (i.e. no compressional component), the magnetosonic modes include both transverse and longitudinal components. The fast and slow modes reduce the plasma pressure gradient while the transverse Alfvén mode reduces the bending of the magnetic field. Since the electric field of the shear Alfvén mode is always perpendicular to the static magnetic field, this mode is almost totally unaffected by the various collisionless damping processes that can exist in a hot, magnetized plasma. Thus, once generated, the waves can propagate great distances with little or no attenuation. A useful analogy to the propagation of the shear Alfvén wave is the propagation of waves on a taut string with the magnetic field providing the tension and the wave energy is transported along the magnetic field lines, as string like oscillations. In contrast, when hot plasma effects are considered, the fast and slow magnetosonic modes always have a small component of the electric field along the static magnetic field, which leads to damping by thermal plasma. From this, it is only the shear Alfvén wave that has the possibility to carry information from the magnetosphere to the ionosphere. Thus, this wave is related to field aligned currents and is often, but not always, associated with micro-pulsations. Finally, the shear Alfvén wave can be seen as the low frequency limit of electromagnetic waves when the ions as well as the electrons are included.

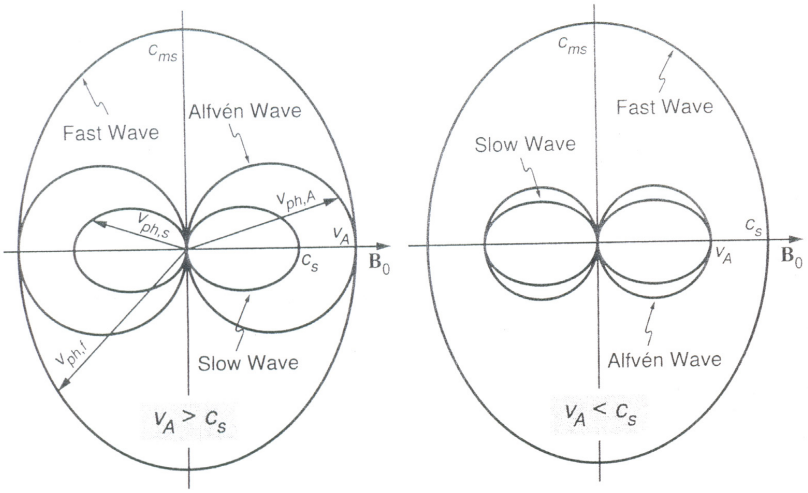

Fig. 9. Phase velocity diagrams of the three MHD wave modes. The annotations seen in the figure corresponds to Alfvén speed (V_A), Sound speed (C_s), Magnetosonic speed (C_{ms}), Background magnetic field ($\mathbf{B}_0$) and Phase velocity for slow- ($V_{ph,s}$), fast- ($V_{ph,f}$) and intermediate Alfvén ($V_{ph,A}$). (From Baumjohann and Treumann, 1997, in Basic Space Plasma Physics.)

An instability never happens as long as the velocity distribution function is Maxwellian, that is when the plasma is in thermal equilibrium. When certain conditions are satisfied, thermal fluctuations of plasma could grow exponentially, and the plasma becomes unstable. Such plasma instabilities occur if some waves grow in intensity or are under conditions far from thermal equilibrium. Plasma waves can grow if the plasma is sufficiently anisotropic, which in turn alters the distribution through wave-particle interaction. Also, when the relative drift velocity between electrons and ions exceeds the local Ion-Acoustic speed, the system is unstable and electrons are heated by excited electrostatic plasma waves. Particle acceleration (as in aurora), wave-particle interaction and wave-wave interaction are all examples that can lead to instability processes that occur regularly in a plasma. In geospace, there are different ways of causing positive feedback from a medium, and some of the most familiar instabilities are the two-stream instability (Farley-Buneman), the gradient drift instability (Rayleigh-Taylor) and the Kelvin-Helmholtz instability. If a stream of electrons and ions differ in velocity by more than the ion-acoustic speed, this two-stream instability produce electrostatic waves that propagate nearly perpendicular to the magnetic field. An example of such instability occurs in the electrojets in the E-region. The gradient-drift instability is also known as the "ExB drift" instability and is analogous to the instability that occurs when a heavier liquid overlies a lighter one. As long as the collision frequency is smaller than the gyro-frequency, the negative electrons and positive ions move in opposite directions when a force is acting at right angles to a magnetic field. If the plasma density in the edge away from the force enhances, a gradient-drift instability may occur. Examples of effective forces are neutral wind or gravity, which may break down irregular structures in the F-region as well as produce structures in injected ion clouds. A typical product of a Kelvin-Helmholtz instability would be the shear Alfvén waves and generation of certain magnetic pulsations in the magnetosphere. It also tends to produce vortices, and the instability often occurs at the interface between two media in relative motion. There the instability depends on the presence of a velocity shear, and it is actually the same instability that causes waves on the surface of water on a windy day.

Incoherent Scatter Technique

In general, the theory of Incoherent Scatter (IS) technique is based on kinetic theory. It only works on charged particles, not on neutrals, and it requires thermal equilibrium. The latter is satisfied when the plasma system's macroscopic thermal state has ceased to change with time, hence the plasma has obtained a stable distribution or temperature through multiple collisions and the energy is shared equally between the various components and their degrees of freedom. The incoherent scatter echo is the result of non-relativistic (Thomson) scattering of electromagnetic energy, radiated from the radar, by electrons in the ionospheric plasma, that are themselves controlled by the much slower and massive positive ions (a proton is 1836 times more massive than a electron). If the electrons are hit by a radar beam, they start to accelerate and accelerated charged particles emit radiation. It is the thermal fluctuation in a medium of short coherence time and a very small cross section (10^{-28} m^2) that is detected, as long as the Bragg criterion is satisfied. For a monostatic radar, using the same antenna for both transmitting and receiving, the Bragg criterion corresponds to structures that match half the size of the incident radiated radar wavelength. At IS radar frequencies ($f_R >> f_p$), the ionosphere is transparent to the radar wave. If the radar frequency is below the plasma frequency, the individual electron fluctuations in the plasma will cancel the electric field of the radar wave. A typical IS radar transmits 1-2 million watts at peak power and only a miniscule fraction is scattered back by the electrons (e.g. 10^{-20} W), and this fraction then has to be collected by a very big antenna.

If the Debye length (λ_D) is larger than the radar wavelength (λ_R), then it is only the information of the motion of each "free" electron that is obtained, and only the electron Thomson scattering that is observed. If the shielding distance is much smaller than the radar wavelength ($(\lambda_D/\lambda_R)^2 << 1$), information about the plasma itself could be obtained as the radar observes the waves scattered by thermal fluctuations of electron density which is described as Ion-Acoustic and Langmuir waves in an unmagnetized plasma. As long as the Debye length is much smaller than the radar wavelength, the IS radar has the possibility to measure Langmuir waves and Ion-Acoustic waves, which are fundamental waves that always exist in plasma due to thermal fluctuations. From all this, a good way to identify plasma in a neutral gas, is by observing high frequency Langmuir waves and/or low frequency Ion-Acoustic waves.

The characteristic IS spectra are double-humped, but below about 100 km the spectra lose their shape and become narrow and single-peaked. This is because the collision between ions and neutrals increases a lot. When the ion-neutral collision frequency (υ_{in}) becomes larger than the Ion-Acoustic frequency (2 – 12 kHz), the Ion-Acoustic waves cannot propagate. If the electron temperature is not much larger than the ion temperature ($T_e/T_i \geq 1$), which is usually the case in the ionosphere above 150 km, the Ion-Acoustic waves are strongly dampened and the spectral lines merge into one broad double-humped line. With small damping, the valley in the ion spectra gets deeper. Accordingly, the depth of the valley between the two Ion-Acoustic shoulders is a measure of the electron to ion temperature ratio. Anomalous IS echoes are radar echoes from the F-region and upper E-region whose ion-line spectral shape departs from that corresponding to thermal equilibrium. Coherent scattering is a sign of instabilities and as long as the temperature ratio between electrons and ions increases, the Ion-Acoustic mode can be appreciably enhanced for values of the streaming electrons much less than the electron thermal speed, and the threshold for the onset of the ion wave instability is greatly reduced.

Figure 10 gives an illustration of an IS spectrum. The information about the plasma can be extracted from the power (density) spectrum [W/Hz], where the ion spectrum represents the power scattered from electrons making up the shielding cloud around the ions, and the motion of this cloud (Doppler broadening) is determined by the ion motion. In general, in the backscatter geometry, the left ion-line peak (left- or downshifted shoulder) and the right ion-line peak (right- or upshifted shoulder), represent Ion-Acoustic waves travelling away and towards the radar, respectively. The IS radar can measure parameters such as i) the electron density from the total power returned from the scattering region (N_e), ii) the line-of-sight ion drift velocity (υ_i, ions bulk motion of a volume) from the Doppler shift of the whole spectra envelope, iii) the electron- to ion temperature ratio (T_e/T_i) from the ratio between the peak and dip, iv) the ion temperature to ion mass ratio (T_i/m_i) from the separation of the peaks, and v) the ion temperature (T_i) and electron temperature (T_e) from the line width of the ion line if the ion mass is known. However, a fitting of the theoretical spectrum to a measured spectrum yields electron density, electron temperature, ion temperature, ion mass and Doppler velocity. In the presence of strong currents, such as relative drift motion between ion and electrons, the IS ion-line spectrum is modified; this makes the spectrum asymmetrical, one ion-peak being higher than the other. Other atmospheric parameters can be further derived indirectly from the routinely derived basic parameters, such as the ion-neutral collision frequency, electric field strength, conductivity and currents, neutral air temperature and wind, exospheric temperature, gravity waves, electron precipitation and associated Joule and particle heating rates. Also, if the electron temperature is already known, plasma parameters such as the electron density could be extracted from the electron plasma line, however, it is much less detectable than ion line. If the plasma line is enhanced it could give information about photo-electrons and electron particle precipitation. Additionally, the presence of photo-electrons produced by solar EUV, can modify the velocity distribution function of the plasma from the Maxwellian. Here the two spectral lines of the so-called down- and upshifted electron plasma line correspond to Langmuir waves travelling away and towards the radar, respectively. The plasma lines could be used to calibrate the radar.

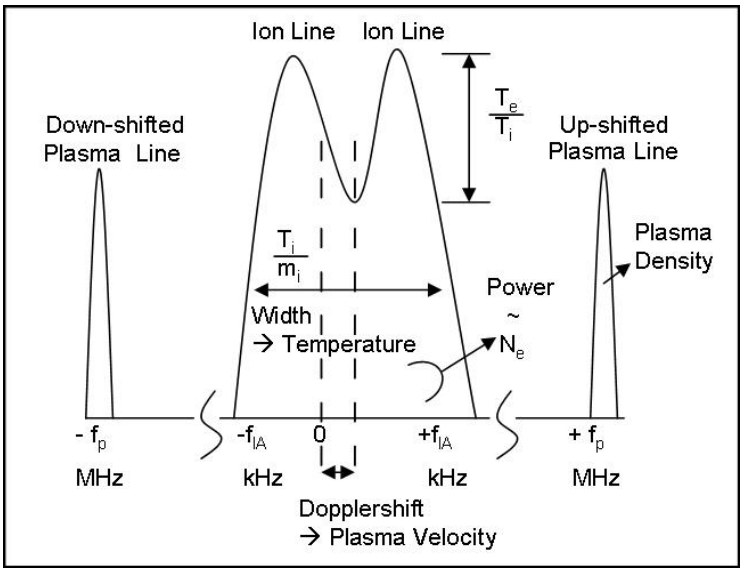

Fig. 10. Typical IS shape of the power density spectrum from F-region.

In order for an IS radar to detect both the plasma- and ion lines, the plasma should be approximately collisionless. This is satisfied whenever the electron-neutral and ion-neutral collision frequencies are much less than the Langmuir- and Ion-Acoustic frequencies, respectively. The latter is often not the case in the E-region. It should be recalled that a radar beam "sees" several Debye spheres, thus, if the plasma varies within any given altitude resolution of the radar, the observations could only give an average of the variations at best. The best choice of radar frequency for the IS technique depends on the scientific aim. Radars of high frequency have trouble measuring plasma waves at high altitudes (> 500 km) owing to the fact that the Debye length in the ionospheric upper F-region increases with altitude. Also, the measurability of small current- and plasma densities is greater by using VHF rather than UHF, while a higher frequency radar is more capable of observing smaller spatial structures due to the Bragg criterion. The VHF EISCAT radar was built to measure at high altitudes (i.e. the polar wind) and in the mesosphere. Longer wavelength allows reaching to higher altitudes with longer Debye lengths. Since only one radar is needed for this purpose, it is possible to build a radar with big antenna. On the other hand, the UHF is optimized to measure below about 500 km, and was built to measure the 3 components of velocity, so 3 antennas were necessary. These two reasons imply a UHF frequency and smaller antennas.

Particle Precipitation

In general, the Earth's magnetic field plays an important role in shielding most of the atmosphere from particle radiation and energetic cosmic rays, but some of the energetic particles end up in the radiation belts which consist of energetic particles that circle around the Earth from about 1000 km and out to 6 times the Earth radius (R_E ~6378 km). Increased Solar wind (plasma) particles which pile up in the boundary between where the Earth's magnetosphere and the interplanetary medium interact (~10 R_E), will also partly protect the Earth from cosmic rays since they increase the plasma around the Earth's magnetosphere, which together with the Earth's magnetic field makes it more difficult for energetic radiation and particles to pass through. From this, solar activity and cosmic radiation are anti-correlated, thus, the amount of cosmic radiation that reaches the Earth is about twice as high during solar minimum than solar maximum. Further down, it is the Earth's atmosphere that protects us from harmful radiation, like ozone (O_3) which absorbs UV radiation in the Hartley band (200 – 300 nm).

It is the initial energy and mass of each particle that decides how far down it could penetrate into the Earth's atmosphere, see Fig. 11. For example, during solar proton events (SPE), which can last for several days, protons of 1 MeV and 100 MeV reach down to ~87 km and ~33 km, respectively. Thus they influence the destruction rate of ozone by increasing the production of HO_x or NO_y in the mesosphere and stratosphere, respectively. Increased production of HO_x has a short time effect (hours) which reduce the ozone by 10% or more while NO_y has a long term effect (months) which reduces the ozone by 1-3%. A SPE (10 protons cm^{-2} s^{-1} sr^{-1} above 10 MeV) can originate from either a solar flare or the interplanetary shock wave driven by a Coronal Mass Ejection (CME), and it could lead to Polar Cap Absorption (PCA). PCA can last for days or weeks, and usually occurs within 48 hours of a SPE. CME (hours, max 96h) are often associated with flares (few minutes), but CME does not cause flares and vice versa. A CME originates in the Sun's outer atmosphere, corona, while flares erupt from the Sun surface close to regions of active sunspots. The main effect of flares is to launch out a wide spectrum of electro-magnetic-energy, but a big flare also releases matter into space, mainly energetic protons. A large solar flare can generate a high flux event of solar cosmic rays, known as solar energetic particle (SEP) event, which lasts typically from

minutes to days, and the proton energies exceed 100 MeV. Both CME and flares disturb the ionosphere and can have dramatic effects on HF-radio propagation. CMEs along with flares can thus disturb radio transmissions, cause power blackouts, and disrupt electrical transmission lines. CMEs can reach 2000 km/s, hence having a higher speed than the solar wind, which on average is about 400 km/s. During halo CME, the entire Sun appears to be surrounded by CME. Most of the time, electrons and protons ejected from the Sun do not reach Earth, and if they do, they do so 20 to 40 hours after the CME. Only 1 of 10 CME shocks hit the Earth. However, it is not the shock wave *per se* that causes the geomagnetic storm, it is the southward B_z that may (or may not) occur in the sheet or the magnetic cloud. If their magnetic orientation is just right, they can disturb the Earth's geomagnetic field and cause a geomagnetic storm.

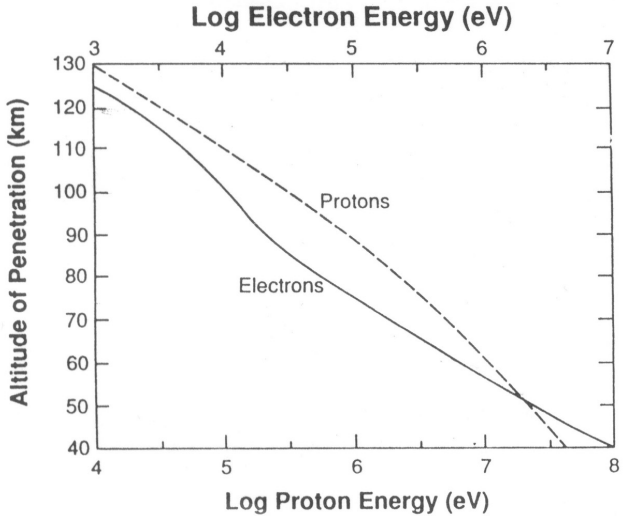

Fig. 11. Stopping altitudes for electrons (1-10^4 keV) and protons (10 – 10^5 keV), in the case of vertical incidence to the atmosphere. (From Luhmann, 1995, in Introduction to Space Physics)

The stopping altitude of an electron also depends on the initial energy of each precipitating electron, for instance: 0.5 keV (180 km), 1 keV (160 km), 2 keV (130 km), 6 keV (110 km) and 100 keV (85 km). As the electron energy increases, the maximum ionization occurs at a lower level in the atmosphere and is also of larger magnitude. From this, electron particle precipitation with energies less than 1 keV, between 1 – 10 keV and more than 10 keV will ionize in the F-, E- and D-region, respectively. Precipitation that penetrates into the D-region enhances the electron density which enhances cosmic noise absorption which is measured by riometers. Since the electron density is always considerably less than the neutral gas density in the upper atmosphere, the precipitating primary electrons collide primarily with the neutrals, and the electrons, in contrast to photons, are not destroyed when they pass through the atmosphere; they become indistinguishable from the ambient thermal electron population when they lose their energy through collisions. Energetic electron precipitation causes a large increase in the electron concentration between 250 – 300 km. It is also possible to have a small increase at about 200 km, as a result of the high energy tail of the precipitating electron spectrum. If increases in the cusp electron concentration at around 150 km are observed, they result from the effects of precipitating ions, rather than electrons.

Particle precipitation such as protons and electrons could either be of Solar or magnetospheric origin. The magnetosphere extends to about 60 000 km (~10 R_E), at the boundary with interplanetary space. There is no sharp boundary between the magnetosphere and the ionosphere, but the boundary can be defined loosely as where charged particles go from being mainly influenced by the magnetic field to being mainly influenced by collisions. From this, in the magnetosphere, the collision frequency is much less than the gyro frequency ($\upsilon << f_g$). The convection cells in the polar cap are the most distinct sign of coupling between the magnetosphere and the ionosphere. Typically, charged particles that stream along the Earth's magnetic field lines are subjected to both inelastic and elastic collisions with the atmospheric constituents, and they lose their energy gradually. Precipitating charged particles in the ionosphere will deposit 40 % of their energy into the atmosphere by ionization and dissociation of atmospheric molecules, 50 % goes into heating and dynamics of the upper atmosphere, while about 10 % of the energy is deposited into very low and extremely low frequency waves (VLF: 3 – 30 kHz and ELF: 0.3 – 3 kHz), as well as excitations in the upper atmosphere like optical aurora and X-ray Bremssthrahlung emission. About 1-2 % is deposited as optical aurora and only a fraction of the precipitating energy will be deposited as Bremssthralung X-rays. The latter is almost exclusively produced by high-energy primary electrons, while the other depositions involve both primary and secondary electrons over a wide range.

Primary auroral electrons that ionize the atmospheric gases, produce secondary electrons that are equivalent to the photo-electrons (~1 - 50 eV) produced by solar EUV radiation. When primary and secondary electrons have collided to the extent that their energy is just above the energy of the thermal electron population, they are termed suprathermal electrons. In addition to precipitating electrons, the latter are also caused by scattering. The transition between thermal and suprathermal influence is usually at rather low energies, below about 2 eV. The energy of suprathermal electrons is shared with the less energetic abundant ambient thermal electrons by elastic collisions, resulting in an increase of the electron temperature. The number of inelastic collision processes in the suprathermal regime is limited to excitation of low vibrational levels or rotational levels in molecules, thus they are also capable of exciting lower excitations levels or states of different atoms. Every ionization event produces a positive ion and a secondary electron and experimental data show that fast electrons and protons produce about one ion-pair (electron-ion) per 36 eV of their initial energy, thus an electron loses ~36 eV on average during each collision. Most of the permitted transitions observed in O (O^+) and N (N^+) have excitation potentials of about 10 – 13 eV (20 – 30 eV). Because the ionization potential of atoms and molecules, on average, is about 15 eV, just less than half of the energy dissipation goes into ionization and more than half of the energy is transferred into the motion (kinetic energy) of the product electron (secondary electron), which subsequently thermalizes while only a few eV go into excitation. Thus, secondary electrons are also able to excite atmospheric atoms and molecules, before ending up as free thermal electrons in the ambient electron gas. Before auroral electrons can produce visible aurora through excited oxygen or nitrogen, they must undergo numerous collisions before their energy is reduced below the average 15 eV to excite an atom. During this process, one auroral particle of for instance 10 keV at the top of the ionosphere, produces about 300 ion-pairs. In order to produce moderately visible aurora, more than 2000 million electrons per cm^2 each second are typically needed if all the electrons have an initial energy of 10 keV. Actually, this means that during one night of auroral activity the precipitating particles easily deliver more than 400 MW (if a horizontal layer with an auroral arc of 1000 km in East-West and 10 km in North-South is assumed). It should then be recalled that it is only 1-2 % of the energy from the precipitating charged particles that will be deposited as optical aurora in the ionosphere.

The excitation energy needed to excite the red (630.0 nm), green (557.7 nm) and blue (427.8 nm) coloured aurora is 1.96 eV for O (^{1}D) state, 4.17 eV for O (^{1}S) state and about 18 eV for N_2^+ (1NG) state, respectively. One electron volt (1 eV) corresponds to the amount of energy an electron gains when accelerated through a potential difference of one volt. Since the excitation of N_2^+ requires the presence of particles whose energies are in excess of 18 eV, the excitation of these emissions is caused mainly by primary particles. If an excited atom collides before its radiative lifetime, all the energy will be deposited onto the colliding particle, or as heat instead being emitted as a photon. One distinguishes between prompt emission and forbidden transitions. Prompt emission means that the excited atom or molecule deposits its energy excess within 100 ns or less, while forbidden transitions have lifetimes greater than 100 ns (10^{-7} s). Both O (^{1}D) and O (^{1}S) are forbidden with a natural lifetime of ~110 s and ~0.75 s, respectively, while N_2^+ (1NG) is a prompt emission. Below 200 km, an O (1D) atom would most likely suffer through a collision that will knock it out of the excited state before it has a chance to emit a photon (quenched), because of the slow transition. However, at higher altitude (300 – 400 km), the 630.0 nm emission could also be excited by thermal excitation (~3000 K). Since the O (^{1}D) level is only 1.96 eV above ground state, it might be possible for thermal electrons to produce excitation, as long as there are enough electrons in the high-energy tail of the thermal distribution for electron temperatures much greater than 3000 K.

The precipitation pattern of auroral particles is aligned by the Earth's magnetic dipole field due to how charged particle motions act in the collisionless magnetosphere. The electron precipitation occurs in distinct regions in the auroral oval, both on dayside (06:00 - 18:00 MLAT) and on nightside (18:00 – 06:00 MLAT), typically when the interplanetary magnetic field (IMF) is southward, $B_z < 0$. The auroral oval is located at higher latitude for daytime aurora than nighttime aurora. Statistically, the typical value for the central geomagnetic latitude on a quiet or moderate day is about 78° +/- 2.5° at noon (12:00 MLT) and 67° +/- 5° at midnight (00:00 MLT), see Fig.12.

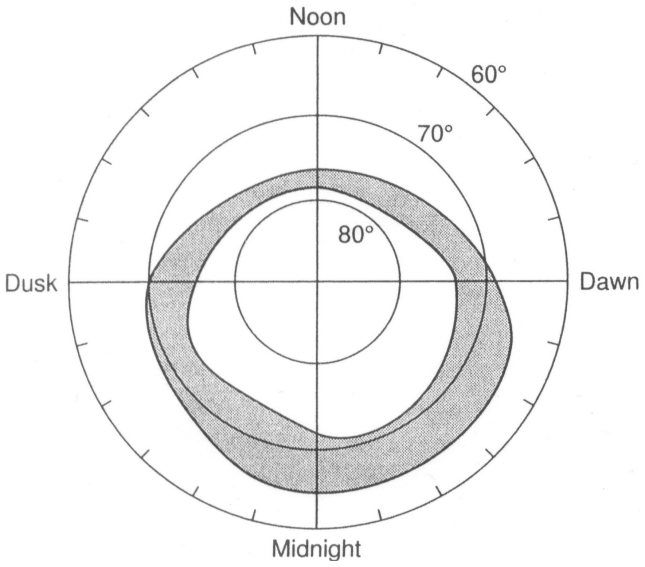

Fig. 12. Average auroral oval. (From Baumjohann and Treumann, 1997, in Basic Space Plasma Physics.)

The polar cap is a circular region poleward of 75° - 80° magnetic latitude, where a connection between the Earth's geomagnetic field and IMF occurs. In this interaction, two neutral points where the total magnetic field is zero are formed on the dayside magnetopause in each hemisphere. The polar cusp is between these points, which typically extend about +/- 1.5 hour from the magnetic noon (10:30 – 13:30 MLT) close to 78° geomagnetic latitude, and are 100 – 200 km deep. However, during very dynamic processes, cusp regions up to +/- 4 hours are possible. Thus, solar wind particles have free entry (Fig. 13) along the open field lines in the cusp, while the auroral emissions equatorward of the cusp are on closed field lines. The auroral oval has a fixed orientation with respect to the sun, and so has the polar cusp, since the latter is a part of the auroral oval, known as the dayside auroral oval.

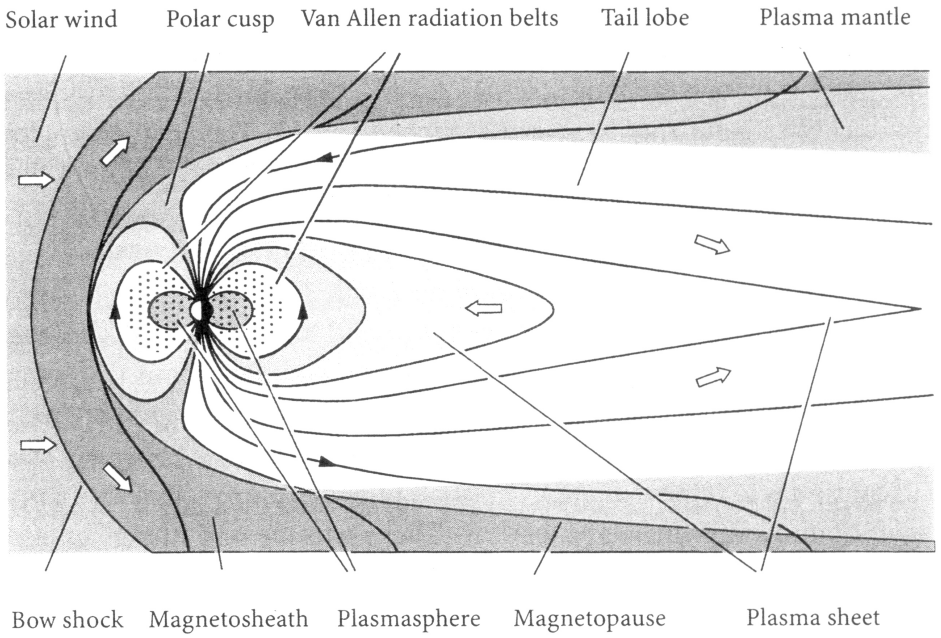

Fig. 13. Polar cusp and plasma circulation. Open arrows indicate the circulation flow of the plasma in this cross-section of the Earth's magnetosphere. Plasma in the solar wind is deflected at the bow shock (left), flows along the magnetopause into the magnetic tail (right), and is then injected back toward the Earth and Sun within the plasma sheet (centre). This plasma circulation pattern is driven by magnetic tension created when the magnetic field in the solar wind merges with that of Earth. This mechanism may provide 80 to 90 percent of the coupling between the solar wind and the Earth's magnetosphere, but solar wind plasma may also enter into other weak points in the Earth's magnetism such as the turbulent bow shock and the polar cusps. (From Lang, 1995, in Sun, Earth and Sky.)

The nightside aurora consists typically of medium energy particles in the energy range of ~0.5 – 20 keV, dominated by particles between 1 and 15 keV, while the dayside aurora is dominated by low-energy particles less than 1 keV, which enter the magnetosphere through the polar cusp. Through satellite measurements it has been found that electrons in the energy range 30 – 100 eV and 70 – 200 eV dominate the cusp and Low Latitude Boundary Layer (LLBL), respectively. Consequently, both the emission heights and spectra differ in the nightside and dayside aurora. In nightside aurora, diffuse and structured auroras are typically seen at altitudes from 100 - 150 km, produced by

particles in the range of 1 – 10 keV. Unstructured aurora occurs at low altitude, below 100 km, produced by medium-energy particles in range of 5 – 20 keV. The height of aurora in the daytime cusp is typically above 200 km (250 km on average). By definition, the dayside cusp aurora is the diffuse band where emission intensity of red line emission (630.0 nm) is much larger than the green line emission (557.7 nm), and is normally observed in the region of 10:30 – 13:30 MLAT. In addition to electron aurora, precipitating protons also give rise to so-called proton aurora. However, this is not visible and it is more diffuse as a result of a large gyro radius and high charge exchange. During geomagnetic storms the amount of protons, H+, increases in the auroral region and decreases in the cusp region.

Finally, as an aside, auroral activity can in addition to visible light also be related to infrasonic waves that travel towards the Earth (Wilson, 1968). These waves are detectable by pressure sensors at ground level, but infrasound is not audible for humans because of the very long wavelengths and frequencies lower than 20 Hz. However, some animals are sensitive to infrasound like giraffes, elephants and whales.

3. CAMPAIGNS AND WORK

This chapter deals with some of the campaigns and unfinished work related to this study. Two of the campaigns attended have played a considerable role in my work, and therefore, a short description of the motivation and framework for these campaigns is included. The unfinished work has been included, since the ideas may be worth following up. The theory about Bremssthrahlung X-ray and cosmic radio noise that is mentioned in one sentence in the theory chapter is given a little more attention here.

ESR/REIMEI Campaign

Background:

ESR/REIMEI was a joint Norwegian-Japanese campaign. The principle instruments were: i) incoherent scatter radar, ESR (EISCAT Svalbard Radar) and ii) a Japanese small satellite, REIMEI (synonymous with 'dawn'). ESR is located in Longyearbyen (78.15°N, 16.03° E GEO & 75.27° N, 111.65° E CGM), ~445 m above sea level and the REIMEI satellite followed a sun-synchronous orbit in the meridian of 12:50 - 00:50 local time at 640 km height. The campaign had duration of 12 days, divided into two periods in 2006; 4 - 9 January and 30 January to 4 February.

Aim of campaign:

This campaign aimed to conduct coordinated observations with high temporal and spatial resolutions of structured aurora, electron precipitation and ion-outflow with ESR and REIMEI satellite in the Earth's polar region. The interest was to study daytime cusp aurora and plasma environments as well as night-time substorm break-up and sun-aligned auroral arcs, if any.

Method:

The campaign was carried out by simultaneous measurements with the ESR and near range passes of the REIMEI satellite. The 32 m antenna pointed at the satellite shortest range direction for about 10 - 15 minutes before/after each pass, elsewhere field aligned. During satellite passes, the radar was run with a code experiment Hilde, and code experiment Steffe when both antennas were field aligned (FA). The satellite carries 3 instruments: i) Multi-spectral Auroral Imager Camera (MAC), ii) Low-energy auroral particle instrument with an Electron and Ion Energy Spectrum Analyzer (EISA) and iii) plasma CuRrent Monitor (CRM).

Result:

Out of 12 days, 8 days were successfully completed with coordinated measurements. In the first campaign period, some problems with the attitude control program on REIMEI caused a spinning mode for the first days, while for the second period, the final day of measuring went wrong due to major failure on the 32 m ESR antenna. From 28 hours of active radar time, the ESR covered 25 Reimei passes, including 3 field-aligned. For scientific results, see Paper III.

RDR/BXR Campaign

Background:

Precipitating electrons deposit their energy into the atmosphere mainly by ionization and heating of the neutral gas. In addition to visible light, a small amount of the energy of precipitating particles in the lower auroral region (E-region) may also be radiated directly as Bremsstrahlung X-rays as the electrons are decelerated. If the precipitation energy at 100 km is above 30 keV, the Bremsstrahlung photons can penetrate to lower altitudes in the atmosphere than the primary electrons themselves. Very few X-rays are produced by secondary electrons, and they are in any case absorbed before exiting into the atmosphere because of their low energy. X-rays at balloon heights (30 – 40 km) are mainly formed by the high energetic tail of auroral particles (> 25 keV), while the optical aurora are mainly due to particles less than 10 keV.

The number of X-ray photons with energies greater than 10 keV generated by an electron with an initial energy slowing down in the atmosphere, is rather small. For example, to produce one photon with energy equal to 10 keV or more, it is on average necessary with 10 electrons with an initial energy (T_0) of 2000 keV, 200 electrons with T_0 = 200 keV, and only 17 500 electrons with T_0 = 20 keV will do the same (Berger and Seltzer, 1972). This means that one electron with initial energy of 2000 keV, 200 keV and 20 keV, deposits 10%, 0.5% and 0.05 ‰ of its energy into Bremsstrahlung X-ray energy, respectively. The great advantage of monitoring Bremsstrahlung is that it is not affected by sunlight, and thus, studies of energetic electron precipitation are not limited to the nightside darkness. In addition, X-rays are insensitive to the atmospheric composition, therefore the X-ray flux produced by a given primary electron distribution is the same, regardless of the altitude distribution of the atmospheric constituents (Robinson and Vondrak, 1994). It is furthermore possible to deduce information from X-rays about the energetic electron precipitation, both spatial distributions and the energy spectrum.

Aim of Campaign:

As part of the Arctic LDB (Long Duration Balloon) program development, the RDR/BXR was a joint Norwegian-Italian student experiment, in corporation with Andøya Rocket Range and the Italian Space Agency (ASI). The objective of the campaign was to have radar measurements (RDR) coordinated with X-ray measurements from the Balloon borne experiment (BXR), which was carried on a 10 000 m^3 ASI stratospheric balloon, to study high energy particle precipitation and associated Bremsstrahlung radiation in the polar atmosphere. The balloon, launched from Longyearbyen, Svalbard, was expected to drift westward, crossing Greenland at a floating altitude of about 35 km. This meant that it was is interesting to operate both the EISCAT Svalbard Radar (78.153°N, 16.029°E geographic coordinates) and the Søndrestrøm radar, to achieve coordinated comparison. The latter is located at Greenland (66.987°N, 309.050°E geographic coordinates). By measuring Bremsstrahlung X-rays with balloon borne instruments and particle precipitation with incoherent radar, simultaneously, it will be possible to study the influence of energetic precipitation on the generation of plasma instabilities, if there is any.

Method:

X-ray fluxes decay very fast below 30 keV because of photoelectric absorption effects due to the X-ray interaction with the gas molecules in the air between the stratosphere and the X-ray production layer (~100 km). Fluxes at higher energies are exposed to multiple Compton scattering. For X-rays in air, photoelectric absorption dominates below about 20 keV (Luhmann, 1976), and fluxes at higher energies than 30 keV are reduced by a factor of 5 -10 at the balloon altitude as an effect of Compton scattering by electrons (Stadsnes, et al., 1997). Compton scattering becomes more important at higher X-ray energies as it scatters photons from lower to higher energies (or vice versa) in interaction with electrons of higher (or lower) energy, hence causing energy degrading of 'secondary' photons. The transport of photons down to balloon heights takes place over large distances, thus the accumulation of soft 'secondary' photons due to multiple Compton scattering is far from negligible. From this, the total X-ray flux near 50 keV could be seriously underestimated when electrons with initial energies equal to, or above, 100 keV are considered (Berger and Seltzer, 1971). However, if the X-rays are generated from electron precipitation with the majority of flux below 40 keV, like typical auroral electron spectra, this underestimation is not so imminent (Luhmann, 1976). Energy reduction through elastic scattering such as Thomson scattering is also possible, but this affects only X-rays less than 10 keV, hence not relevant for balloon borne measurements. Yet, this could be important for measurements carried out above 100 km, like instruments on satellites or rockets.

A useful energy range for a balloon borne X-ray detector will be between 30 keV up to 100 keV, where the spectrum is expected to peak at energies between 40 and 50 keV. The effective detector area should be greater or equal to 2 cm^2, in order to have sufficient counts/second. In this student experiment, YAP scintillators together with a photomultiplier are used. The active detection area is about 4 cm^2, with an expected 1000 – 2000 counts/second during disturbed geomagnetic activity. Because of the low partial pressure at the balloon height, which typically varies between 3 – 6 hPa, it was important to seal the high voltage part with silicon compound to avoid corona discharge. Despite the relatively cold temperatures in the stratosphere, the instrument box should be coloured in such a way that the sunlight would be reflected instead of absorbed. Thus, the instrument box should be white rather than black, in order to prevent the instrument from being depreciated by increased heat inside the box.

Operational Result:

The balloon was successfully launched from Longyearbyen Airport (78.247°N, 15.465°E geographic coordinates) on 14 June 2006 at 14:56 UT and terminated above Greenland on 1 July at 23:06 UT. The balloon flew westward in a circumpolar trajectory between 77° N and 81° N at about 35 km floating level (~ 6 g/cm^2). In general, with less sunlight, the balloon would descend, but during midnight sun this is not a large problem. While passing areas of pack ice, reflection from ice and snow contributes to increased temperature. Hence, the balloon floated a bit higher than 35 km. The variations in altitude were within 28 and 37 km. About 2 hours after launch, the balloon reached an altitude of 36 km and became stable. The ESR (EISCAT Svalbard Radar) was operated for 7 hours: i) 2006-06-14 between 16:00 – 21:00 UT and ii) 2006-06-15 between 06:45 – 08:55 UT.

During the radar run with code experiment Hilde, the 32 m antenna was pointed at the corresponding field aligned position for the balloon at 300 km. The balloon was floating above Svalbard and within the radar range for 15 hours. After 2 days the balloon reached

the east coast of Greenland and on the 17 June at 08:00 UT, the position was 79.151°N, 305.56°E, which is north of the Søndrestrøm radar. The range between the balloon and the site was 1400 km at 6º antenna elevation, hence no measurements were taken because the latitude was too far north and the elevation angle was too low. The X-ray instrument was communicating, and data was streaming in real time. Additionally, a riometer located in Longyearbyen was operational. Unfortunately, when possible interesting geophysical activity occurred above Svalbard, recorded by riometer and/or X-ray instrument, the ESR was not in operation or the balloon was out of range, hence, no results of scientific value were achieved. However, a presentation of the campaign was held at COSPAR 2008 and a popular science article has been published, see appendix C.

Unfinished Work: Cosmic Noise Absorption vs. NEIALs

The following work has been done in collaboration with Peter Stauning, Danish Meteorology Institute (DMI). Despite that the work is no way complete; it does contain significant points for reflection.

Background:

In general, a common physical parameter for both NEIAL and Cosmic Noise Absorption (CNA) observations is the enhanced electron density. It should therefore be worthwhile to look closer into this, in particular, regarding the influence by particle precipitation. Lunde et al. (2007) discussed the possibilities of hard particle precipitation (> 500 eV) present during NEIAL events on 22 January 2004. There were indications of this seen in the riometer (relative ionospheric opacity meter), magnetometer data, and optical data with strong intensities in both 427.8 nm and 557.7 nm optical lines. In this work, we will follow up the discussion by comparing more selected days of NEIAL events to riometer measurements. Even though only a few events may match, we believe that it is still valuable, and may give a better understanding of the geophysical surroundings. At least, it should be possible to indicate whether the case study from 22 January 2004 was only a single coincidence or not.

Cosmic Noise Absorption (CNA):

Stellar sources in the galaxy radiate broadband radio frequency. The riometer technique for examining electron density enhancements in the ionosphere is based on absorption of this cosmic radio noise (Little and Leinbach, 1959). Measurements are typically made at frequencies between 20 – 50 MHz, since the radio wave absorption at these frequencies is sensitive to overall changes in electron density in the ionospheric regions. Radio wave absorption in the upper atmosphere is mostly related to the enhanced ionization caused by energetic particle precipitation, caused by collisions between electrons and heavier particles such as ions or neutrals. The absorption intensity depends on both electron density and collision frequency. Also enhanced electron temperatures caused by strong electric fields are a contributor to absorption events, as variations in the electron temperature may cause changes in the collision frequency. The so-called Auroral absorption (~1 dB or more) is caused by energetic electron precipitations (> 10 keV) from the magnetosphere, which increase the ionospheric electron density between ~70 and 120 km (Detrick and Rosenberg, 1990). It is not only energetic electrons that cause CNA, protons of 100 keV or 1MeV penetrate to heights of 110 km and 80 km, respectively, and may cause cosmic noise absorption there as well. In addition, proton bombardment could partly contribute to slowly varying (morning) absorption (SVA), which always occurs in the morning hours (08 MLT) under locally quiet geomagnetic conditions, but

most of the absorption is due to ionization by electrons. SVA are recognised by a smooth increase in absorption by as much as 8 dB for about 30 minutes, and thereafter absorption diminishing over several hours. According to Stauning (1997), the height ranges for the active absorption regions spans from: i) 200-400 km for F-region disturbances, ii) 90 -120 km for E-region electron heating events, iii) 70-100 km for most substorm associated events, and iv) 50-80 km during polar cap absorption events with energetic protons (1 – 100 MeV) and electrons (0.1 – 10 MeV). As for cosmic noise absorption, several classes have been defined, and a further description of these can be found in Stauning (1996a).

IRIS:

IRIS (an acronym for Imaging Riometer for Ionospheric Studies) is located in Adventdalen, Svalbard (78.20° N, 15.80° E geographically and 74.21° N, 131.53° E geomagnetic, 1995). The riometer operates at a frequency of 38 MHz within a protected radio-astronomy band. The system consists of 64 single parallel dipole elements, with a half wavelength separation between each dipole. They are configured into 8x8 narrow beams, by using a Butler matrix phasing system. At a height of 90 km, the field of view (FOV) corresponds to 240 km x 240 km at either side of zenith, and at 300 km, the FOV equals to 600 km x 600 km. The absorption of the cosmic noise signals are measured by comparing the riometer output voltage (proportional to the input RF power) with the quiet day diurnal voltage, after this has been corrected for sidereal time difference. Thereafter, the ratio is converted into decibel units. The sensitivity of the instrument is 0.1 dB, limited by the bandwidth (B) in Hertz and integrated time constant (τ) in seconds. CNA can be found by the basic formula: Absorption = $-10 \cdot \log (P/P_O) = 10 \cdot \log \{1 + [2 (\tau \cdot B)^{-1}]^{0.5}\}$, where P and P_O are perturbed signal power and undisturbed (quiet level) power, respectively (Detrick and Rosenberg, 1990). Since the ionospheric absorption efficiency differs with the operational frequency, a multiplication factor of $1.6(38^2/30^2)$ should be added to the calculated absorption values, if comparing results from a 38 MHz riometer against a 30 MHz riometer (Stauning et al., 1995b). The horizontal spatial resolution is 25 km close to the centre (less at the edges), and the system scan through all the 64 beams in about 80 ms, and 12 scans are averaged to produce one integrated image every second.

Method:

In this study, a suitable undisturbed level, Quite Day Curve (QDC), is chosen for each specific time of day, since QDC varies. In general, QDCs represent the cosmic noise power received from galactic noise source in one day but also depend on seasonal variation, solar zenith angle, time of day, chemical composition etc. However, if a high value of QDC is recorded, it is most likely due to a strong local interference (yielding upward irregular deflections). Strong scintillations in connection to a discrete noise source, such as Cassiopeia-A or Cygnus-A, will typically be blanked out in the dataset. These signals are coherent, in contrary to ordinary cosmic background noise. However, before being blanked out, they should be studied in detail to see if there is any valuable information after all. This ought to be done because not all scintillations are related to discrete radio sources; they could also contain other information, such as turbulence in the ionosphere. When wavelike structures in the ionosphere appear, like regular density variations in the F-region, signals with slightly different propagation could interfere, either constructively or destructively and thus result in large amplitude variations, which can be seen as scintillations. The mechanism that induces the formation of wave structures in the ionosphere is not well known, but horizontal electric field is believed to play an important role (private communication Peter Stauning).

Discussion:

Even though the dominant cause of high-latitude absorption events is still considered to be the variable high-energy electron particle precipitation, various processes other than this may cause enhanced ionospheric radio-wave absorption as well. Absorption events in the daytime sector at cusp latitudes which rarely exceed 0.5 dB (at 30 MHz), could be related to increased electron collision frequencies caused by electron temperature enhancement (Stauning, 1984). Such elevated electron temperatures are associated with E-region plasma instabilities generated by strong ionospheric electric fields, and subsequently strong currents. Another weak absorption is due to polar convection disturbances (Stauning, 1998), while disturbances associated with strong convection shear may cause enhanced and strongly variable precipitation of the eastward drifting high-energy electrons accelerated during substorm activity (Stauning et al., 1995a). Enhanced plasma convection with a strong electric field (> 25 mV/m) causes Farley-Buneman plasma instability in the E-region, thus electron heating and the electron-to-neutral collision frequency increase, which again may cause CNA (Stauning, 1997). Short-lived (1-3 min) small-scale absorption events of 100-200 km in extent, superposed on large-scale absorption features extending ≥ 700 km in longitude have been associated with impulsive magnetic variations (Nishino et al., 1997). Sudden precipitation of high energy magnetospheric electrons (30 -300 keV) at high latitudes, can cause daytime absorption (0.2 – 0.3 dB) spike events of 1-2 minutes duration (Stauning et al., 1996). In the F-region, a combination of high density and low electron temperatures leads to high electron to ion collision frequencies which could cause CNA, and absorption above 180 km has been associated with plasma patches (Rosenberg et al., 1993; Nishino et al., 1998). All this means that it is not always straightforward to find the unambiguous source which causes the observed CNA.

Preliminary result:

A selection of NEIAL events observed at ESR has been compared with coincident evaluated IRIS data: 1998-01-21, 1998-01-24, 1998-06-21, 2000-11-26, 2000-11-27, 2002-01-17, 2002-06-09, 2002-06-10, 2003-01-26, 2004-01-22, 2004-11-07 and 2006-01-23. All IRIS data are obtained from the riometer located in Longyearbyen, except the data from 22 January 2004; where data from the riometer located in Ny Ålesund were used because data from the Longyearbyen riometer were not available. Furthermore, all IRIS data from Longyearbyen have been distributed and evaluated by Peter Stauning, Danish Meteorological Institute (DMI). In addition to the already published result from 22 January 2004, at least 3 more clear cases of cosmic noise absorption could be seen at 2000-11-26, 2000-11-27 and 2004-11-07. It should be noted that during these 3 events, as well as the 2004-01-22, CME activities were present. These results at least show that the case study from 22 January 2004 was not a single coincidence. Possible weak fluctuating absorption has also been found in the dataset, at least on 2006-01-23. However, the cause of weak absorption is not clear, but a possible explanation could be: i) Precipitation of substorm-associated electrons having diffused out to boundary field lines, ii) Splash of soft electrons involved in field aligned currents (FACs), iii) High F-region electron densities (surprisingly, daytime F-region electron densities are sometimes higher in winter than in summer) and iv) E-region turbulence and instabilities in high electric fields (personal communication with P. Stauning). Not all the data sets have been evaluated adequately; this in particular applies to the scintillation problem.

4. SUMMARY AND CONCLUSION

The 5 papers presented in this study have one common denominator: particle precipitation at high latitudes. The driving force behind the campaigns attended was to attain coordinated observations during occurrences of natural enhanced ion acoustic lines. The probability for this to happen was small, but it was worth trying. Even though the campaigns did not succeed in measuring plasma instabilities like NEIALs, the outcome of each campaign can be termed a success based on other findings. The participation in the different campaigns has provided access to a large number of observations and data from different observational platforms, and has resulted in a number of peer reviewed papers. The ESR data used in the study of NEIALs were extracted from the EISCAT database. A summary of each papers conclusion is presented below. Additionally a short over all conclusion of how these papers are linked together as well as suggestion of possible future projects regarding NEIALs are introduced.

Summary of Papers

Paper I:

J. Lunde, B. Gustavsson, U. P. Løvhaug, D. A. Lorentzen, and Y. Ogawa: *Particle precipitations during NEIAL events: simultaneous ground based observations at Svalbard, Ann. Geophys., 25, 1323 – 1336, 2007.*

This paper presents Natural Enhanced Ion Acoustic Lines observed during cusp hours with the EISCAT Svalbard Radar, based on more than 50 events within an hour. The study includes simultaneous data from meridian scanning photometer, magnetometer and riometer. The large numbers of observed NEIALs together with observations from the additional ground-based instruments enabled the possibilities to gain some characteristics of the particle precipitation and auroral intensity coupled to the observations such as: i) the intensity of the red line (630.0 nm) as well as other lines must be above a certain minimum, ii) the characteristic energy typically exceeds 50 eV, iii) the particle energy flux exceeds 3.4 mW/m^2, iv) large intensity ratio between red and green line (630.0/557.7 >> 5), v) disturbance in the magnetic field as the horizontal component reaches a maximum excursion of ~380 nT about 10 minutes prior to the first NEIAL, vi) *K*-index equal or larger than 5, and vii) occurrence of cosmic noise absorption. The results indicate that NEIALs were accompanied by energetic particles from the high energy tail in addition to the typically soft electron precipitation (< 500 eV).

Paper II:

T. Grydeland, B. Gustavsson, L. Baddeley, J. Lunde, and E. M. Blixt: *Conditional integration of Incoherent Scattering in relation to flickering aurora*, J. Geophys. Res.,113, A08305, doi:10.1029/2008JA013039, 2008.

This paper presents results from co-ordinated measurements with a high-speed narrow field-of-view Optical Digital INstrument (ODIN) and the EISCAT Svalbard Radar. It is the incoherent scatter (IS) radar observations of the ionospheric response to particle precipitation causing flickering aurora that are presented. The study demonstrates a new conditional integration technique for incoherent scatter radar in relation to flickering aurora, by integrating pulses at the same phase as the optical white light intensity variation in the field aligned direction. This method makes it possible to study

ionospheric responses at short time-scales (10 to 100 ms). It was also found that IS backscatter power was exposed with a modulation factor of about 3% in amplitude, which could be explained with electron heating caused by temporally modulated electron precipitation and electron cooling in collisions with ions and neutrals.

Paper III:

J. Lunde, S. C. Buchert, Y. Ogawa, M. Hirahara, K. Seki, Y. Ebihara, T. Sakanoi, K. Asamura, M. Okada, T. Raita, and I. Häggström: *Ion-dispersion and rapid electron fluctuations in the cusp: a case study*, Ann. Geophys., 26, 2485-2502, 2008.

This paper presents results from co-ordinated measurements with the low altitude REIMEI satellite and the EISCAT Svalbard Radar, together with other ground-based instruments. The results are mainly related to the dayside cusp where clear signatures of ion-dispersion were seen in the satellite data: 3 distinct steps in the ion energy and at least 2 more steps as well. In addition, the paper deals with fast variations of the electron flux and energy which occur during the events of ion dispersion. It has been demonstrated that the majority of the observed cusp structured ion-dispersions are most likely related to magnetopause reconnection, produced in an intermittent state by temporal cusp features rather than a stationary one. The small-scale (< 5 km) and fast electron fluctuations (< 1s) were also found to be most probably due to the reconnection process.

Paper IV:

B. Gustavsson, J. Lunde, and E. M. Blixt: *Optical observations of flickering aurora and its spatio-temporal characteristics*, J. Geophys. Res., 113, A12317, doi:10.1029/ 2008JA013515, 2008.

This paper presents optical observations of flickering aurora measured with a high-speed narrow field-of-view imager in white light. The flickering aurora is usually characterised by optical emissions varying in intensity with frequencies typically between 5 and 15 Hz. Both the intensity variation and apparent motion of the flickering spots have been studied. The amplitude of the intensity variations was found to be 10% while the frequency was between 5 and 12 Hz. The characteristic patterns found were compared with the spatial patterns derived from interference between electromagnetic ion-cyclotron waves. The flickering spots displayed clear drifts and rotational motions as well as more complicated patterns. By extending the Sakanoi-Temerin model from one to two dimensions and allowing for interference between four EMIC-waves, spatial patterns could be derived. These derived spatio-temporal patterns agreed very well with the observed flickering aurora.

Paper V:

J. Lunde, U. P. Løvhaug, and B. Gustavsson: *Particle precipitation during NEIAL events: simultaneous ground based nighttime observations at Svalbard*, Ann. Geophys., 27, 2001 – 2010, 2009.

This paper presents for the first time, Natural Enhanced Ion Acoustic Lines observed during night-time hours with the EISCAT Svalbard Radar, together with auroral emissions observed with the meridian scanning photometer. This study shows, in contrary to previous studies, that the NEIALs are not always associated with enhanced red line intensity larger than 10 kR, and even more important, in one of the events, the

green line intensity exceeds the red line. Compared with paper I, this paper also shows a clear negative deflection of ~425 nT in the horizontal magnetic field component about 10 minutes before the first NEIAL observations, *K*-index larger than 5, characteristic energy larger than 50 eV, while the energy particle flux greater than 2.4 mW/m^2 was somewhat less. Finally, this paper suggested that the 844.6 nm emission line could be a good candidate as an optical signature for NEIALs rather than the 630.0 nm emission, due to the fact that the former is a prompt emission while the latter is not.

Conclusion

As the summary of each paper shows, they all contribute to an increased knowledge of the main theme of this thesis: particle precipitation. The individual papers deal with specific subjects; but they also supplement each other. Interestingly, all the observations could have happened during the same time period, because the phenomena; i) dispersion, ii) flickering aurora and iii) NEIALs are all associated with particle precipitation. In that respect, the papers are effectively linked together. Furthermore, the distribution of energetic and less energetic particles has a direct influence on i), ii) and iii). Another common point is that all these phenomena are more likely to occur during high geomagnetic activity. These papers may contribute to a better understanding of how the energy from the Sun is deposited and redistributed in the Earth's upper polar atmosphere through particle precipitation. This could lead to a better further understanding of how the deposit of energy from particle precipitation is connected to climatic and atmospheric dynamics. Finally, both flickering aurora and large ion-acoustic waves (NEIALs) could cause serious problems for satellite navigation and communication in Polar Regions, and therefore they should make a valuable object for future studies.

Possible Future Projects

There is still a lot of science that can be done to get a better understanding how particle precipitation affects its ionospheric surroundings, and in particular how it relates to NEIALs. First of all, it could be interesting to test whether NEIALs are associated with broad band electrostatic noise (BEN) or not, since bursts of BEN have been recorded in the dayside auroral region (e.g. Dubouloz et al., 1991a and 1991b). BEN spans over a wide range of frequencies, from below 10 Hz and up to the local electron plasma frequency. It is already known that type III solar radio bursts are associated with Langmuir waves. Electrons ejected by a solar flare produce a bump-on-tail distribution because of time of flight considerations, thereby causing the growth of Langmuir waves in the solar wind. This cannot be detected directly from the Earth; however these plasma oscillations produce electromagnetic radiation, generated by non-linear interactions at and twice the plasma frequency (Ginzburg and Zhelezniakov, 1958) that can be detected from Earth, and are known as type III solar burst which are recognized by a decreasing frequency with increasing time.

NEIALs could be associated with Alfvénic motion along the magnetic field. A common understanding is that low frequency magneto-acoustic waves, such as shear Alfvén waves, may be the cause of particle acceleration that produces aurora. From this, Alfvén waves will cause field aligned currents (aurora), and if the currents are strong enough, they may well be associated with NEIALs. When such a current is present, a double hump is produced in the equivalent reduced velocity distribution function, and this double hump can lead to the growth of ion-acoustic waves, and the ion-acoustic mode can then be driven unstable. From this, downward propagation Alfvén waves may

directly cause the generation of upward and downward ion-acoustic waves, and if they are exposed to large disturbances, this could lead to NEIALs. During large fluxes of low energy electrons (0.1 – 1 keV), Alfvén waves are capable of producing small-scale (<< 1 km) visible auroral structures, and the current densities associated with these waves are found to be very large (Chaston et al., 2003). Therefore, this could be of interest regarding the two stream current instability theory.

Another relation with NEIALs that should be investigated closer, is the association with CME activity, and especially the accompanying alpha-proton ratio which under undisturbed conditions varies between 0.005 - 0.04. During investigated NEIAL events (not published), this ratio exceeded 0.04, hence indicating that alpha particles could be of importance. The alfa-ratio flux is in general of importance for characteristic energies below 400 eV. It is well known that large amounts of protons (H^+) are a signature of reconnection, and on average, the proton energy flux represents about 15% of that of electrons. Thus, maybe the next step regarding NEIAL studies should not only be concentrated on the electron precipitation. It could also be worthwhile to identify the thermal (kinetic) to magnetic pressure at the bow shock, to see if this ratio somehow has an influence on possible NEIAL events.

NEIALs in the E-region have not been reported to any great extent, but have been observed at 126 km in association with meteor trails. By looking at the decay time of the density or temperature enhancement, it should be possible to identify NEIALs in the E-region also (discussed with Bjørn Gustavsson). If the decay time to "normal" level is much faster than a corresponding recombination time, this indicates that the plasma is not thermal but a probable NEIAL event. Some other ideas for future projects could be a coordinated campaign with ESR and a balloon borne IR-camera, this makes it possible to study aurora during daylight together with NEIALs.

Besides the mentioned suggestions, it might be worth while to follow up on the investigation already started regarding K-index, negative H-component, characteristic energy, energy particle flux, soft and hard precipitation, emission intensities and so on.

As a final remark, it should be remembered that "a theory is scientific only if it is *falsifiable* (Popper)".

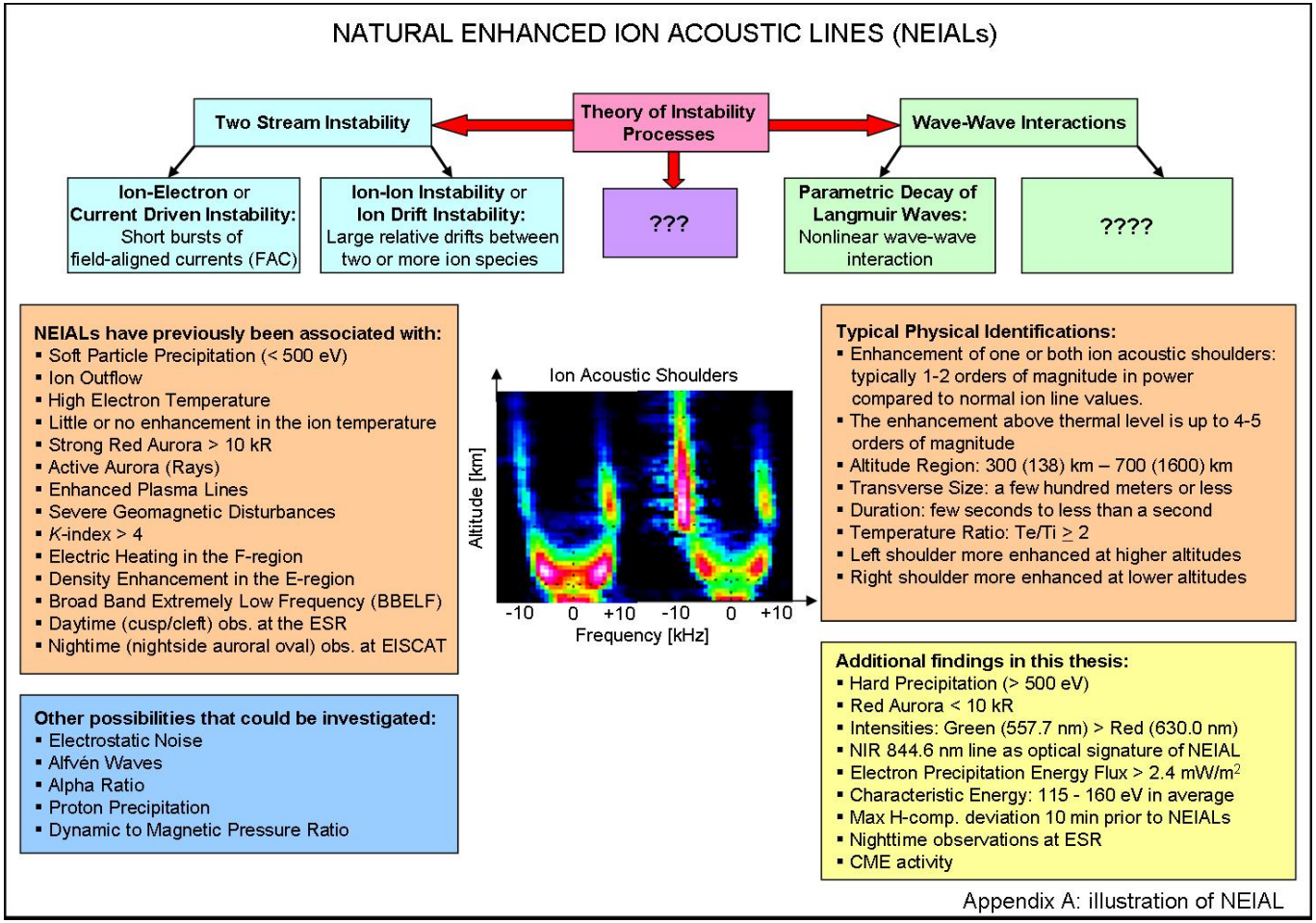
NATURAL ENHANCED ION ACOUSTIC LINES (NEIALs)
Two Stream Instability
Theory of Instability Processes
Wave-Wave Interactions
Ion-Electron or Current Driven Instability: Short bursts of field-aligned currents (FAC)
Ion-Ion Instability or Ion Drift Instability: Large relative drifts between two or more ion species
???
Parametric Decay of Langmuir Waves: Nonlinear wave-wave interaction
????
NEIALs have previously been associated with:
▪ Soft Particle Precipitation (< 500 eV)
▪ Ion Outflow
▪ High Electron Temperature
▪ Little or no enhancement in the ion temperature
▪ Strong Red Aurora > 10 kR
▪ Active Aurora (Rays)
▪ Enhanced Plasma Lines
▪ Severe Geomagnetic Disturbances
▪ K-index > 4
▪ Electric Heating in the F-region
▪ Density Enhancement in the E-region
▪ Broad Band Extremely Low Frequency (BBELF)
▪ Daytime (cusp/cleft) obs. at the ESR
▪ Nightime (nightside auroral oval) obs. at EISCAT
Ion Acoustic Shoulders
Altitude [km]
-10 0 +10 -10 0 +10
Frequency [kHz]
Typical Physical Identifications:
▪ Enhancement of one or both ion acoustic shoulders: typically 1-2 orders of magnitude in power compared to normal ion line values.
▪ The enhancement above thermal level is up to 4-5 orders of magnitude
▪ Altitude Region: 300 (138) km – 700 (1600) km
▪ Transverse Size: a few hundred meters or less
▪ Duration: few seconds to less than a second
▪ Temperature Ratio: Te/Ti ≥ 2
▪ Left shoulder more enhanced at higher altitudes
▪ Right shoulder more enhanced at lower altitudes
Other possibilities that could be investigated:
▪ Electrostatic Noise
▪ Alfvén Waves
▪ Alpha Ratio
▪ Proton Precipitation
▪ Dynamic to Magnetic Pressure Ratio
Additional findings in this thesis:
▪ Hard Precipitation (> 500 eV)
▪ Red Aurora < 10 kR
▪ Intensities: Green (557.7 nm) > Red (630.0 nm)
▪ NIR 844.6 nm line as optical signature of NEIAL
▪ Electron Precipitation Energy Flux > 2.4 mW/m²
▪ Characteristic Energy: 115 - 160 eV in average
▪ Max H-comp. deviation 10 min prior to NEIALs
▪ Nighttime observations at ESR
▪ CME activity
Appendix A: illustration of NEIAL

Appendix B: Illustration of Method

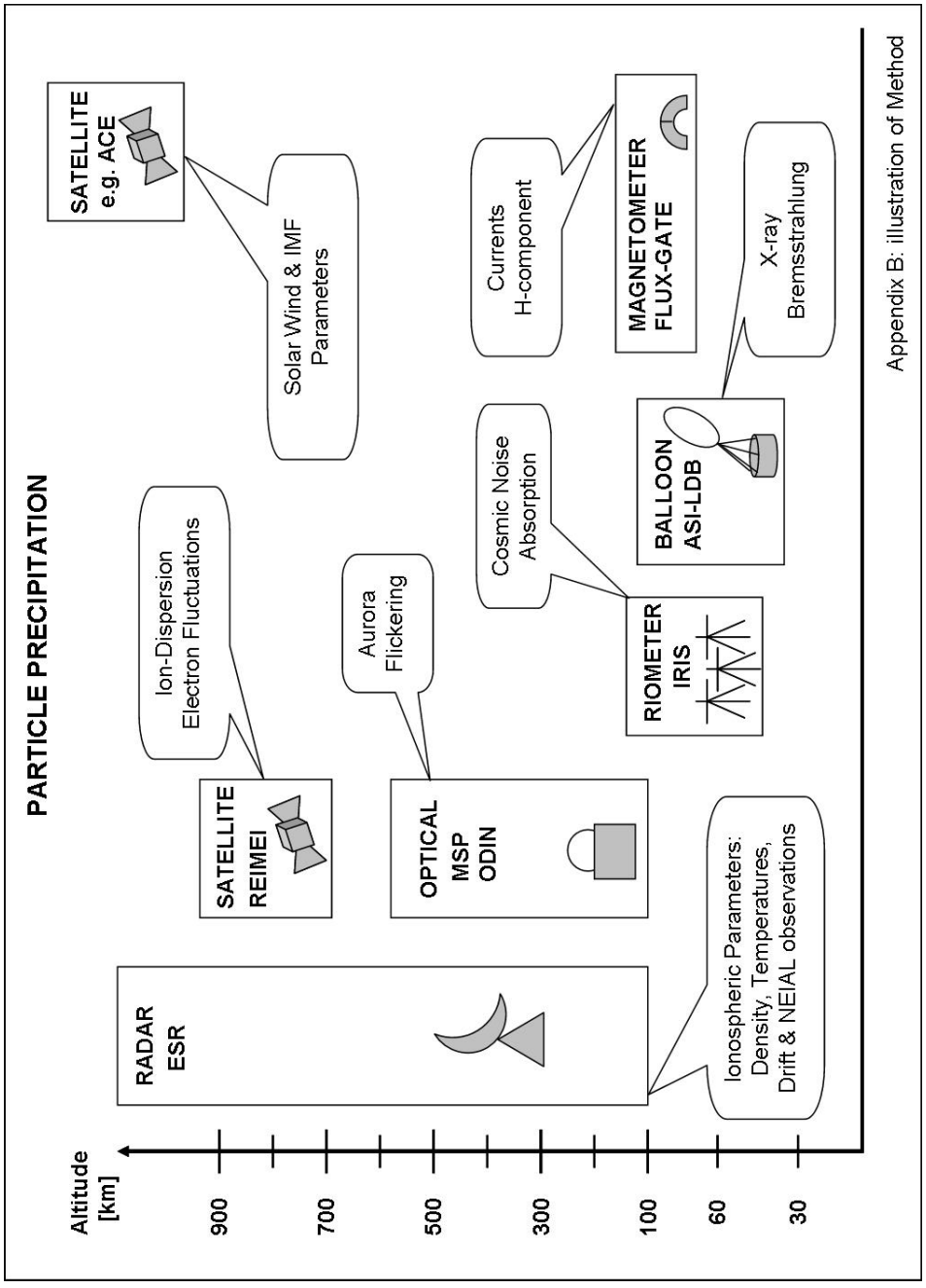

Appendix C: RDR/BXR

Romforskning med Ballonger

Av June Lunde

Ballonger, hvem har vel ikke et forhold til ballonger? I utallige former og farger, er de til stor glede for mange, liten som stor. Foruten vannballonger, som har en tendens til å ende med et "plask", er det noe befriende og forunderlig, det å se en ballong stige høyt til værs. At ballonger viser seg å egne seg ypperlig til bærere av vitenskaplige instrumenter, er en desto større fornøyelse!

Ballonger i vitenskap

Ballonger er kanskje ikke det man først og fremst forbinder med romforskning. De er som skilpadder å regne sammenliknet med fartsfylte raketter, ei heller svever de så høyt som satellitter og romsonder. Men, nettopp her ligger deres styrke; de beveger seg i et høydeområdet som ellers er utilgengelige, de driver langsomt over store områder, og de er relativt billige. Dette gjør dem til en viktig og utfyllende del av romvirksomheten. Mulighetene er

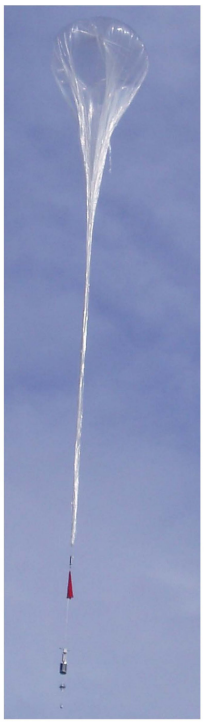

Ballongen er sluppet! Fra topp til bunn: ballongen, søker, avkoplingsenhet, fallskjerm (rød), antenne til navigasjon (GPS) og kommunikasjon (IRIDIUM), nyttelast, ballast, solpanel, radarreflektor og til slutt et magnetometer.

Trykket i ballonghøyden er over 100 ganger lavere enn ved jordoverflaten og temperaturen er lav. Nyttelasten er innkapslet i en tett boks for å beskytte mot det lave trykket. Tross minusgrader, er det allikevel nødvendig å beskytte instrumentet mot at det blir for varm! Enkleste måte å forhindre dette, er å male alt hvitt. Da vil innfallende varmestråling fra sola bli reflektert.

mange, det er bare fantasien som setter grenser. Vitenskaplige instrumenter plassert på ballonger egner seg godt til å studere stråling fra sola og verdensrommet, magnetiske avvik og vindsystemer med mer. Dette igjen kan være med å bidra til nyttige resultater innen områder som biomedisin, navigasjon og klimaforskning.

Store er de

Størrelsen avhenger av formålet, ønsket svevehøyde og ikke minst vekten til alle instrumentene som skal løftes opp (nyttelast). Små ballonger med volum på 10 000 kubikkmeter vil typisk være utstyrt med 10 kg nyttelast, mens de 10 ganger større mellomstore ballongene vil kunne løfte flere hundre kg. Å legge ut en liten ballong krever bredden av fotballbane mens en mellomstor ballong vil kreve hele lengden. De største ballongene som finnes, er over 1 million kubikkmeter. Det er store greier, selv en fotballbane blir for liten i denne sammenheng. Disse kan løfte flere tonn med utstyr. Her holder det ikke med manuell muskelkraft, tunge kranbiler kreves. Selve materialet består av syltynn gjennomsiktig plast. Dette er veldig slitesterkt i utvidelsesretning, men er sårbart for rifter. Selv den minste rift er ødeleggende. Alle skarpe gjenstander er tabu under et ballongslipp, hvite "servitør" hansker blir tatt i bruk.

Ballongslipp

Før et slipp overhodet vurderes, må bakkevinden kontrolleres grundig. Det skal ikke store vindpustet til før det hele må avlyses. Etter at ballongen er lagt pent ut på en "løper", fylles den opp med heliumgass (som har en massetetthet som er 7 ganger mindre enn luft). Selve ballongslippet er spennende, det er mye som skal klaffe. Etter at ballongen er sluppet, stiger den relativt raskt opp til 40 km høyde. Deretter daler den litt og vil typisk stabilisere seg rundt 35 km høyde, dette tar omtrent et par timer. Her svever den høyt over alle skyer, helt fri for forstyrrelser fra flytrafikk. Under ferden kan den både stige og synke litt, alt ettersom den blir utsatt for mye eller lite sol. Den kan også stige litt dersom den passerer store områder med pakkis, da refleksjoner fra snø og is ved jordoverflaten bidrar til økt varme. Om ballongen synker litt for mye ned, er det mulig å regulere dette med å kvitte seg med litt ballast (små vekter som frigjøres ved hjelp av en liten kruttladning). Hvor fort ballongen forflytter seg avhenger av høydevinder. Med moderate høydevinder vil hastigheten typisk være mellom 1 5 m/s, men med kraftige høydevinder vil farten fint kunne overstige 10 m/s. Ballongen kan sveve i flere dager og dens ferd avsluttes kontrollert ved hjelp av en fjernstyrt kruttladning som aktiveres. Nyttelasten vil da bli frigjort fra ballongen og dale ned i en fallskjerm.

Hva måler vi?

I sommer ble det gjennomført et vellykket ballongslipp fra Longyearbyen, Svalbard. Universitetet i Tromsø fikk mulighet til å ha med en vitenskaplig nyttelast gjennom et samarbeid med Andøya Rakettskytefelt og det italienske romsenteret (ASI). Ballongferden varte i hele 18 dager, og

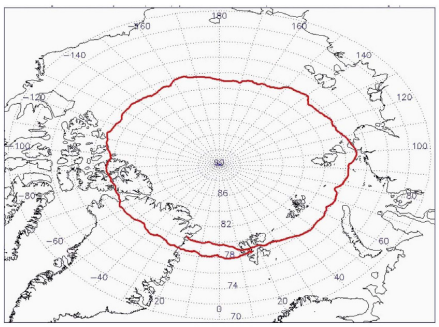

Ruten til ballongen som ble sluppet fra Svalbard i juni i sommer. Den drev over en hel runde rundt polen før den ble tatt ned over Grønland.

litt mer enn en runde rundt nordpolen ble tilbakelagt. Selve studenteksperimentet bestod av et røntgenstråleinstrument, hvor hensikten var å studere "røntgennordlys". Når partikkelnedbør bremses opp i jordens øvre atmosfære (ionosfæren), vil dette kunne generere røntgenstråling i en høyde rundt 100 km. Partikkelnedbør er elektriske partikler med høy hastighet som slynges ut fra solen, også kjent som solvind. Partiklene i solvinden strømmer ned langs jordens magnetfelt og kolliderer med jordens øvre atmosfære. Største delen av partiklenes energi går med til oppvarming, mens noe går med til å skape nordlys og en enda mindre del til røntgenstråling. Denne røntgenstrålingen er ikke mulig å studere fra bakken på grunn av spredning og absorpsjon i atmosfæren, man må opp i en høyde på minst 30 km. Ballonger egner seg derfor ypperlig til å studere "røntgennordlys".

Romvirksomhet uten ballonger kan sammenliknes med et barneselskap eller tivolibesøk uten ballonger; det er gøy, men kunne vært enda kjekkere!

Det matematisk-naturvitenskapelige fakultet (MNF) er et av Universitetets seks fakulteter. MNF omfatter på sin side seks institutter (biologi, fysikk/teknologi, geologi, informatikk, kjemi og matematikk/statistikk) samt Tromsø geofysiske observatorium. Forskere ved MNF vil i tiden framover presentere resultater og betraktninger fra sitt arbeide. Det er en kjent sak at nasjonen rekrutterer for lite realister. Det er vårt håp at artiklene vil vekke nysgjerrighet og interesse for realfagen generelt, og spesielt for de aktiviteter vi har ved MNF.
Professor Tore O Vorren,
Dekan ved MNF.

June Lunde er utdannet flytekniker ved Luftforsvarets Tekniske Skolesenter og Sivilingeniør i Romteknologi ved Høgskolen i Narvik. For tiden er hun ansatt som stipendiat i Romfysikk ved institutt for Fysikk og Teknologi.

Ionosphere

Scale Height in Neutral Gas, H [m]:
$H = k_B T / m g$

Mean Free Path, l [m]:
$l = 1/\sigma_s n = \upsilon v_{r.m.s}$

Lorentz-Force on a single particle, $\mathbf{F}_L$ [N]:
$\mathbf{F}_L = q\mathbf{E} + q\mathbf{v} \times \mathbf{B}$

Gyro/Larmor Radius, r_g [m]:
$r_{ge} = (m_e v_{e\perp} / B q) = v_{e\perp} / \omega_{ge}$
$r_{gi} = (m_i v_{i\perp} / Z B q) = v_{i\perp} / \omega_{gi}$

Gyro/Cyclotron Frequency, f_g [Hz]:
$f_{ge} = 2\pi^{-1} (B q / m_e)$, $f_{gi} = 2\pi^{-1} (Z B q / m_i)$

Angular Gyro-Frequency, ω_g [rad/s]:
$\omega_g = 2\pi f_g = r_g^{-1} (2 k_B T/m)^{1/2}$

Ambipolar Diffusion Coefficient, D_a:
$D_a = k_B (T_e + T_i) / (m_e \upsilon_{en} + m_i \upsilon_{in})$

Electron/Ion Diffusion Coefficient: D_e, D_i:
$D_e = k_B T_e / m_e \upsilon_e$ $D_i = k_B T_i / m_i \upsilon_{in}$

Electron-Ion Collision Freq., υ_{ei} [s^{-1}]:
$\upsilon_{ei} \approx 3.62$ E-6 $n_i T_e^{-3/2} \ln \Lambda$

Electron-Neutral Collision Freq, υ_{en} [s^{-1}]
$\upsilon_{en} \approx 5.4$ E-10 $n_n T_e^{1/2}$

Electron Collision Frequency, υ_e [s^{-1}]
$\upsilon_e \equiv \upsilon_{en} + \upsilon_{ei}$

Ion-Neutral Collision Freq., υin [s-1]
$\upsilon_{in} \approx 2.6$ E-15 $(n_n + n_i) (M'_n)^{-1/2}$

Temperature

Total Particle Velocity, $\mathbf{v}$-$\mathbf{u}_s$ [m/s]:
$\mathbf{v}$ = Velocity of an individual particle
$\mathbf{u}_s$ = Average velocity of a collection of particles, bulk flow

Average speed, $\langle \mathbf{v}\text{-}\mathbf{u}_s \rangle$ [m/s]:
$\langle \mathbf{v}\text{-}\mathbf{u}_s \rangle = (8 k_B T / \pi m)^{1/2}$

Root mean square velocity, $v_{r.m.s}$ [m/s]:
$v_{r.m.s} = (3 k_B T/m)^{1/2}$

Most Probable Thermal Speed, v_{Ts} [m/s]:
$v_{Ts} = (2 k_B T/m)^{1/2} = (2gh)^{1/2}$

Thermal Energy, W [J]:
$(\langle m_s(\mathbf{v} - \mathbf{u}_s)^2 \rangle)/2 = (N k_B T_s)/2$

Kinetic Energy, E_k [eV]:
$E_k = (3/2) (T/11605)$ When N = 3

Thermal Equilibrium:
$m_1 \langle v_1^2 \rangle = m_2 \langle v_2^2 \rangle$

Escape Velocity, v_{esc} [m/s]:
$v_{esc} = (2 G M/r_c)^{1/2}$ $g = G M/R_E$

Joule Heat Dissipation [W/m^2]:
$q_J(z) = \mathbf{j} \mathbf{E} = \sigma_P(z) E_\perp^2$

Energy Units, $W = k_B T$

	J	K	eV	erg
1 J	-	7.24E22	6.24E18	1E7
1 K	1.38E-23	-	8.62E-5	1.38E-16
1 eV	1.60E-19	1.16E4	-	1.60E-12
1 erg	1E-7	7.24E15	6.24E11	-

Particle Precipitation

Energy of Radiation, E [J]:
$E = h f = h c / \lambda$
E[eV] = 1.240E-6/λ

Current Density, $\mathbf{j}$ [A/m^2]:
$\mathbf{j} = n_e q (\mathbf{v}_i - \mathbf{v}_e) = \sigma(\mathbf{E} + \mathbf{v} \times \mathbf{B})$

Ionospheric Current, $\mathbf{j}$ [A/m^2]:
$\mathbf{j} = \sigma_P \mathbf{E}_\perp - \sigma_H (\mathbf{E}_\perp \times \mathbf{B}/B) + \sigma_\parallel \mathbf{E}_\parallel$

Plasma Conductivity, σ_0 [S/m]:
$\sigma_\parallel = \sigma_0 = n_e q^2 / m_e \upsilon$ Birkeland
$\sigma_P = \sigma_0 (\upsilon^2 / (\upsilon^2 + \omega_{ge}^2)$ Pederesen
$\sigma_H = - \sigma_0 (\omega_{ge} \upsilon / \upsilon^2 \omega_{ge}^2)$ Hall

Cowling Conductivity, σ_c [S/m]:
$\sigma_c = \sigma_P + \sigma_H^2 / \sigma_P$ (Eq. Electrojet)

Auroral Conductivity, Σ [S/m]:
$\Sigma_A = \Sigma_P + \Sigma_H^2 / \Sigma_P$ (Auroral Electrojet)

Electron Aurora:
$X + e \rightarrow X^* + e'$
$X^* \rightarrow X + h\nu$ (auroral photons)

$X + e \rightarrow (X^+)^* + e_n + e'$
$(X^+)^* \rightarrow X^+ + h\nu$ (auroral photons)

e: precipitating primary electron
X: atom/molecule (e.g. N, O,)
X: molecule (e.g. N_2, N_2^+, O_2, O_2^+)
$^+$ ionised and * excited
e' = e – 36 eV
e_n: secondary electron (ends up as a free thermal electron)

Plasma

Electron Plasma Frequency, ω_{pe} [Hz]:
$\omega_{pe} = (n_e q^2 / m_e \varepsilon_0)^{1/2}$ $f_{pe} = \omega_{pe}/2\pi$

Ion Plasma Frequency, ω_{pi} [Hz]:
$\omega_{pi} = (n_i Z^2 q^2 / m_i \varepsilon_0)^{1/2}$ Z = 1 for protons

Debye Length, λ_D, λ_{De}, λ_{Di} [m]:
$\lambda_{D,eff} = \lambda_{De}\lambda_{Di}/(\lambda_{De}+\lambda_{Di})$ $\lambda_D = (k_B T_e \varepsilon_0 / n_0 q^2)^{1/2}$
$\lambda_{De} = (k_B T_e \varepsilon_0 / n_e q^2)^{1/2}$ $\lambda_{De} = 69.1(T_e/n_e)^{1/2}$
$\lambda_{Di} = (k_B T_i \varepsilon_0 / n_i q^2)^{1/2}$

Number of electrons in a Debye Sphere, N_D:
$N_D = (4\pi/3)\, n_e \lambda_{De}^3 = 1.37\ E6\ (T^{3/2}/n_e^{1/2})$

Coulomb cut-off Parameter, Λ :
$\Lambda = 12\pi n_e \lambda_{De}^3 = 9 N_D$

Magnetic Pressure, $p_m = B^2/2\mu_0$
Kinetic Pressure, $p_k = n k_B T$

Thermal-to-Magnetic Ratio,Plasma Beta, β:
$\beta = (n k_B T)/(B^2/2\mu_0)$

Electron Thermal Speed, $v_{th,e}$ [m/s]:
$v_{th,e} = (k_B T_e / m_e)^{1/2}$ @ 1AU ≈ 1500 km/s
$v_{th,e} = \omega_{pe} \lambda_{De}$

Ion Thermal Speed, vth,i [m/s]:
$v_{th,i} = (k_B T_i / m_i)^{1/2}$ @ 1AU ≈ 35 km/s
$v_{th,i} = \omega_{pi} \lambda_{Di}$

If $\omega_r >> \omega_p$: Thermal Velocity, v_{th} :
$v_{th,e} = (2 k_B T_e / m_e)^{1/2}$
$v_{th,i} = (2 k_B T_i / m_i)^{1/2}$

Plasma Scale Height, H_p [m]
$H_p = 2H$ (above F-region peak density)

Waves in Plasma

Wave Phase Velocity, v_{ph} [m/s]:
$v_{ph} = \omega/k = f\lambda$ $k = 2\pi/\lambda$ (wavenumber)

Speed of Light, c [m/s]:
$c^2 = 1/\mu_0\varepsilon_0$

Speed of Sound, C_s [m/s]:
$C_s = (\gamma p_0/\rho_0)^{1/2} = (\gamma k_B T/m)^{1/2}$

Ion-Acoustic (Sound) Speed, C_{ia} [m/s]
$C_{ia} \equiv ((\gamma_e k_B T_e + \gamma_i k_B T_i)/m_i)^{1/2}$ γi =3 (adiabatic)
$C_{ia} = (k_B(T_e + 3T_i)/m_i)^{1/2}$ γe =1 (isothermal)

Alfvén Speed, V_A [m/s]
$V_A = B/(\mu_0 n m)^{1/2}$ $\rho_m = n_i m_i$

Magnetosonic Speed, C_{ms} [m/s]:
$C_{ms} = C_s + V_A$

Light Wave (electromagnetic):
$\omega = (\omega_{pe}^2 + k^2 c^2)^{1/2}$ no DC magnetic field

Langmuir Plasma Wave, ω_l (electrostatic):
$\omega_l = \omega_{pe}(1 + \gamma_e k^2 \lambda_{De}^2)^{1/2}$ $\gamma_e = 3$ (adiabatic)
$\omega_l = (\omega_{pe}^2 + \gamma_e k^2 v_{th,e}^2)^{1/2}$

Ion-Acoustic Wave, ω_{ia} (electrostatic):
$\omega_{ia} = k C_{ia} / (1 + k^2 \lambda_{De}^2)$
$\omega_{ia} = k C_{ia} / (1 + (k^2 C_{ia}^2/\omega_{pi}^2))^{1/2}$

Shear Alfvén Wave, ω_A (electromagnetic):
$\omega_A = k V_A \cos\theta$ $\omega_A = k_\parallel V_A$ if $k^2 << \omega_{pi}2/c^2$

Magnetosonic Wave, ω_{ms} (electromagnetic):
$\omega_{ms} = k_\perp C_{ms}$ (Fast) if $V_A << c$
$\omega_{ms} = k_\parallel V_A$ (Fast), $\omega_{ms} = k_\parallel C_s$ (Slow) if $V_A > C_s$
$\omega_{ms} = k_\parallel C_s$ (Fast), $\omega_{ms} = k_\parallel V_A$ (Slow) if $V_A < C_s$

Incoherent Scatter Technique

Radar Wavelength, λ_R [m]:
$\lambda_R = c / f$

Transversal Resolution, Δ_{tr} [m]:
Δ_{tr} = Distance x sin θ
θ = 70*λ_R/aperture diameter

Radial Resolution, Δ_{rr} [m]:
$\Delta_{rr} = c\, t_{tx}/2$
t_{tx} = transmitter pulse length

Maximum Range, R_{max} [m]:
$R_{max} = c / 2$ PRF
PRF = Pulse Repetition Frequency

Bragg Criterion: $n\lambda_R/2 \sin(\varphi/2)$

Electron Density, n_e:
$n_e = \sigma_e / (1 + (T_e/T_i))\, S_c$
Power $\propto n_e$
$\omega_{pe} \propto (n_e)^{1/2}$

Ion Acoustic Frequency, f_{IA}[Hz]:
$f_{IA} \approx (k_B(T_e + 3T_i)/m_i)^{1/2}$ $(2f_R/c)$

Doppler Shift, Δf_i
$\Delta f_i = ((8 k_B T_i/m_i)^{1/2} / \lambda_R$

Doppler Shift, Δf_e,
$\Delta f_e = f_{pe}(1 + 12\pi^2 \lambda_{De})^{1/2}/0.5\lambda_R$

If large υ_{in} → single peaked ion line:
Ion Line Width $\propto T/m_i \upsilon_{in} \lambda_R^2$

Physical Denomination

λ	Wavelength in meter, [m]
f	Frequency in Hertz, [Hz]
υ	Collision frequency in Hertz, [Hz]
T	Temperature in Kelvin, [K]
M	Mass in kilogram, [kg]
h	Height in meter, [m]
W	Thermal energy in Joule, [J]
E_k	Kinetic energy in electron Volt, [eV]
B	Magnetic field strength in Tesla, [T]
E	Electric field strength in Volt m^{-1},[V/m]
J	Current density in Ampere m^{-2}, [A/m^2]
σ_s	Cross section for collisions, [m^2]
Σ	Conductivity in Siemens pr. meter [S/m]
n_n	Number density of neutrals, [m^{-3}]
n_i	Plasma density of ions, [m^{-3}]
n_e	Plasma density of electrons, [m^{-3}]
M'_n	Mean neutral molecular mass, [kg]
M	Mass of the planetary body, [kg]
ρ_0	Density, [kg/m^3]
p_0	Pressure, [Pa] (1Pa = $1N/m^2$)
N	Number of spatial "degrees of freedom"
ω/k	Dispersion relation, [m/s]
n	Integer
Σ	Sum
γ	Ratio of specific heat, adiabatic constant
Z	Atomic number H(1), He(4), O(16)
ln Λ	For most plasma in the range 8 – 25, for estimation of collision freq., assume ~10
S_c	System correction factor.

Physical Constants

c_0	Speed of light in vacuum	2.998 E8 m/s
g	Earth's gravitational acc.	9.807 m/s^2
h	Planck's constant	6.626 E-34 J s
k_B	Boltzmann's constant	1.381E-23 J/K
amu	Unified atomic mass unit	1.661 E-27 kg
m_e	Rest mass of electron	9.109 E-31 kg
M_p	Rest mass of proton	1.673 E-27 kg
m_p/m_e	Proton/electron mass ratio	1836
σ_T	Thomson scat. cross section	6.652 E-29 m^2
μ_0	Permeabilty of free space	4π E-7 H/m
ε_0	Permittivity of free space	8.85 E-12 F/m
q	Electron charge	1.602 E-19 C
eV	Electron Volt	1.602 E-19 J
G	Gravitational constant	6.673 E-11 N m^2/kg^2

Other Physical Miscellaneus Values

R_E	Mean radius of the Earth	6376 km
M_E	Mass of Earth	5.980 E24 kg
M_S	Solar mass	1.989 E30 kg
R_S	Mean Solar radius	6.960 E8 m
1 AU	One Astronomical Unit	1.496 E11 m
E_e	Solar constant at 1AU	1380 W/m^2
1R	Rayleigh	1E6 photons/cm^2 s column
B_{eq}	Mean magnetic field	30 319 nT
B_p	Polar magnetic field	61 000 nT 1T = Wb/m^2
H	Earth's neutral atmosphere mean scale height at surface	8.430 km

BIBLIOGRAPHY

Akasofu, S.-I. and Kamide, Y.(Eds.): *The Solar Wind and the Earth, Terra Scientific Publ. Co., printed in Japan*, ISBN 90-277-2472-5, 1987.

Baumjohann, W. and Treumann, R. A.: *Advanced Space Plasma Physics, Imperial College Press, printed in Singapore*, ISBN 1-86094-026-9, 1997.

Baumjohann, W. and Treumann, R. A.: *Basic Space Plasma Physics*, Imperial College Press, printed in Singapore, ISBN 1-86094-079-X, 1997.

Bellan, M. B.: *Fundamentals of Plasma Physics*, Cambridge University Press, printed in U.K., ISBN 13 978-0-521-82116-2, 2006.

Berger, M. J. and Seltzer, S. M.: *Bremsstrahlung in the Atmosphere*, J. Atmos. Terr. Phys., 34, 85-108, 1972.

Bittencourt, J. A.: *Fundamentals of Plasma Physics*, 3rd, Springer-Verlag New York, printed in USA, 2004.

Boyd, T. J. M. and Sanderson, J. J.: *The Physics of Plasmas*, Cambridge University Press, printed in USA, ISBN 978-0-521-45012-9, 2003.

Brekke, A.: *Physics of the Upper Polar Atmosphere*, Praxis publishing Ltd, printed in Great Britain, ISBN 0-471-96018-7, 1997.

Chaston, C.C., Peticolas, L. M., Bonnell, J. W., Carlson, C. W., Ergun, R. E., McFadden, J. P., and Strangeway, R. J.: *Width and brightness of auroral arcs driven by internal Alfven waves*, J. Geophys. Res., 108, doi: 10.1029/2001JA007537, 2003.

Chen, F. C.: *Introduction to Plasma Physics and Controlled Fusion*, 2nd, Plenum Press, New York, printed in USA, ISBN 0-306-41332-9, 1994.

Detrick, D. L. and Rosenberg, T. J.: *A phased-array radiowave imager for studies of cosmic noise absorption*, Radio Sci., 25, 325-338, 1990.

Duboin, N. –L. and Kamide, Y.: *Latitudinal variations of Joule heating due to the auroral electrojets, J. Geophys.*, Res., 89, 245-251, 1984.

Dubouloz, R. Pottelette, R., Malingre, M., and Treumann, R. A.: *Generation of broadband electrostatic noise by electron acoustic solitons*, Geophys. Res. Lett., 18 155-158, 1991a.

Dubouloz, R. Pottelette, R., Malingre, M., Holmgren, G., and Lindqvist, P. A.: *Detailed Analysis of Broadband Electrostatic Noise in the Dayside Auroral Zone*, J. Geophys. Res., 96, 3565-3579, 1991b.

Ginzburg, V. L. and Zhelezniakov, V.V: *On the Possible Mechanisms of Sporadic Solar Radio Emission (Radiation in an Isotropic Plasma),* Astron. Zhur., 35, 694, 1958.

Giraud, A. and Petit, M.: *Ionospheric Techniques and Phenomena*, D. Reidel, Dordrecht Publishing Co., printed in Holland, ISBN-10 9027704996, 1978.

Glatthor, N. and Hernandez, R.: *Temperature anisotropy of drifting ions in the auroral F-region*, observed by EISCAT, J. Atmos. Terr. Phys., 52, 545-560, 1990.

Gurnett, D. A. and Bhattacharjee, A.: *Introduction to Plasma Physics*, Cambridge University Press, printed in U.K., ISBN 0-521-36730-1, 2005.

Hargreaves, J. K.: *The Solar-Terrestrial Environment*, Cambridge University Press, printed in Great Britain, ISBN 0-521-32782-2, 1992.

Hays, P. B., Jones, R. A., and Rees, M. H.: *Auroral heating and the composition of the neutral atmosphere,* Planet Space Sci., 21, 559-573, 1973.

Houghton, J.: *The Physics of Atmospheres*, Cambridge University Press, printed in U.K., ISBN 0-521-01122-1, 2002.

Kivelson, M. G. and Russel, C. T.: *Introduction to Space Physics*, Cambridge University Press, printed in USA, ISBN 0-521-45714-9, 1995.

Kleinknecht, K.: *Detectors for Particle Radiation*, Cambridge University Press, printed in U.K., ISBN 0-521-64854-8, 1998.

Lang, K. R.: *Sun, Earth and Sky*, Springer-Verlag Berlin Heidenberg, printed in Germany, 1995.

Little, C. G. and Leinbach, H.: *The riometer – a device for continuous measurements of ionospheric absorption*, Proc. IRE, 47, 315-320, 1959.

Luhmann, J. G., *Auroral bremsstrahlung spectra in the atmosphere*, J. Atmos. Terr. Phys., 39, 595-600, 1977.

McCrea, I. W., Lester, M., Robinson, T. R., Wade, N. M., and Jones, T. B.: *On the identification and occurrence of ion frictional heating events in the high-latitude ionosphere*, J. Atmos. Terr. Phys., 53, 587-597, 1991.

Nishino, M., Yamagashi, H., Stauning, P., Rosenberg, T. J., and Holtet, J. A.: *Location, spatial scale and motion of radio wave absorption in the cusp-latitude ionosphere observed by imaging riometers*, J. Atmos. Solar-Terr. Phys., 95, 903-924, 1997.

Nishino, M., Nozawa, S., and Holtet, J. A.: *Daytime ionospheric absorption features in the polar cap associated with poleward drifting F-region plasma patches*, Earth Planet Space, 50, 107-117, 1998.

Nygrén, T.*: Introduction to Incoherent Scatter Measurements*, Invers Publication, printed in Finland, ISBN 951-97489-0-3, 1996.

Robinson, R. M. and Vondrak, R. R.: *Validation of techniques for space based remote sensing of auroral precipitation and its ionospheric effects*, Space Sci. Rev., 69, 331-407, 1994.

Rosenberg, T. J., Wang, Z., Rodger, A. S., Dudeney, J. R., and Baker, K. B.*: Imaging riometer and HF radar measurements of drifting F region electron density structures in the polar cap*, J. Geophys. Res., 98, 7757-7764, 1993.

Schunk, R. W. and Nagy, A. F.: *Ionospheres: Physics, Plasma Physics, and Chemistry*, Cambridge University Press, printed in U.K., ISBN 0-521-60770-1, 2000.

Stadsnes, J., Aarsnes, K., and Bjordal, J.*: X-ray Imaging of the Aurora*, Adv. Space Res., 20, 1043-1054, 1997.

Stauning, P.: *Absorption of cosmic noise in the E-region during electron heating events. A new class of riometer absorption events*, Geophys. Res. Lett., 11, 1184-1187, 1984.

Stauning, P., Clauer, C. R., Rosenberg, T. J., Friis-Christensen, E., and Sitar, R.: *Observations of solar-wind-driven progression of interplanetary magnetic field By-related dayside ionospheric disturbances*, J. Geophys. Res., 100, 7567-7585, 1995a.

Stauning, P., Yamagishi, H., Nishino, M., and Rosenberg, T. J.: *Dynamics of Cusp-Latitude Absorption Events Observed by Imaging Riometers*, J. Geomag. Geoelectr., 47, 823-845, 1995b.

Stauning, P.: *Investigations of ionospheric radio wave absorption processes using imaging riometer techniques*, J. Atmos. Terr. Phys., 58, 753-764, 1996.

Stauning, P. and Rosenberg, T. J.: *High-latitude daytime absorption spike events*, J. Geophys. Res., 101, 2377-2396, 1996.

Stauning, P.: *Ionospheric Investigations Using Imaging Riometer Observations*, In: Review of Radio Science 1993 – 96, ed. W. Ross Stone, 585-617, Oxford University Press, 1997.

Stauning, P.: *Polar convection-related ionospheric radiowave absorption processes observed by imaging riometers*, Adv. Space Res., 22, 1279-1288, 1998.

Suess, S. T. and Tsurutani, B. T.: *From the Sun*, American Geophysical Union, printed in USA, ISBN 0-87590-292-8, 1998.

Wilson, C. R.: *Infrasonic waves from moving auroral electrojets*, Planet. Space Sci., 17, 1107-1120, 1969.

Paper I

Particle precipitations during NEIAL events: simultaneous ground based observations at Svalbard.

Ann. Geophys., 25, 1323 – 1336, 2007.

Paper II

Conditional integration of Incoherent Scattering in relation to flickering aurora.

J. Geophys. Res.,113, A08305, doi:10.1029/2008JA013039, 2008.

Paper III

Ion-dispersion and rapid electron fluctuations in the cusp: a case study.

Ann. Geophys., 26, 2485-2502, 2008.

Paper IV

Optical observations of flickering aurora and its spatio-temporal characteristics.

J. Geophys. Res., 113, A12317, doi:10.1029/2008JA013515, 2008.

Paper V

Particle precipitation during NEIAL events: simultaneous ground based nighttime observations at Svalbard.

Ann. Geophys., 27, 2001 – 20010, 2009.

June Lunde

Particle Precipitation: Effects on Selected Ionospheric Phenomena

2009

LUNDBLADMEDIA AS, TROMSØ

ISBN 978-82-8236-012-8